Rate Constants for OH with Selected Large Alkanes: Shock-Tube Measurements and an Improved Group Scheme

R. Sivaramakrishnan and J. V. Michael*

Chemical Sciences and Engineering Division, Argonne National Laboratory, Argonne, Illinois 60439

Received: December 12, 2008; Revised Manuscript Received: February 19, 2009

High-temperature rate constant experiments on OH with the five large (C_5-C_8) saturated hydrocarbons *n*-heptane, 2,2,3,3-tetramethylbutane (2,2,3,3-TMB), *n*-pentane, *n*-hexane, and 2,3-dimethylbutane (2,3-DMB) were performed with the reflected-shock-tube technique using multipass absorption spectrometric detection of OH radicals at 308 nm. Single-point determinations at ~1200 K on *n*-heptane, 2,2,3,3-TMB, *n*-hexane, and 2,3-DMB were previously reported by Cohen and co-workers; however, the present work substantially extends the database to both lower and higher temperature. The present experiments span a wide temperature range, 789−1308 K, and represent the first direct measurements of rate constants at $T > 800$ K for *n*-pentane. The present work utilized 48 optical passes corresponding to a total path length of ~4.2 m. As a result of this increased path length, the high OH concentration detection sensitivity permitted pseudo-first-order analyses for unambiguously measuring rate constants. The experimental results can be expressed in Arrhenius form in units of cm^3 $molecule^{-1}$ s^{-1} as follows:

$$k_{OH+n\text{-heptane}} = (2.48 \pm 0.17) \times 10^{-10} \exp[(-1927 \pm 69\ K)/T] \quad (838-1287\ K)$$
$$k_{OH+2,2,3,3\text{-TMB}} = (8.26 \pm 0.89) \times 10^{-11} \exp[(-1337 \pm 94\ K)/T] \quad (789-1061\ K)$$
$$k_{OH+n\text{-pentane}} = (1.60 \pm 0.25) \times 10^{-10} \exp[(-1903 \pm 146\ K)/T] \quad (823-1308\ K)$$
$$k_{OH+n\text{-hexane}} = (2.79 \pm 0.39) \times 10^{-10} \exp[(-2301 \pm 134\ K)/T] \quad (798-1299\ K)$$
$$k_{OH+2,3\text{-DMB}} = (1.27 \pm 0.16) \times 10^{-10} \exp[(-1617 \pm 118\ K)/T] \quad (843-1292\ K)$$

The available experimental data, along with lower-*T* determinations, were used to obtain evaluations of the experimental rate constants over the temperature range from ~230 to 1300 K for most of the title reactions. These extended-temperature-range evaluations, given as three-parameter fits, are as follows:

$$k_{OH+n\text{-heptane}} = 2.059 \times 10^{-15} T^{1.401} \exp(33\ K/T)\ cm^3\ molecule^{-1}\ s^{-1} \quad (241-1287\ K)$$
$$k_{OH+2,2,3,3\text{-TMB}} = 6.835 \times 10^{-17} T^{1.886} \exp(-365\ K/T)\ cm^3\ molecule^{-1}\ s^{-1} \quad (290-1180\ K)$$
$$k_{OH+n\text{-pentane}} = 2.495 \times 10^{-16} T^{1.649} \exp(80\ K/T)\ cm^3\ molecule^{-1}\ s^{-1} \quad (224-1308\ K)$$
$$k_{OH+n\text{-hexane}} = 3.959 \times 10^{-18} T^{2.218} \exp(443\ K/T)\ cm^3\ molecule^{-1}\ s^{-1} \quad (292-1299\ K)$$
$$k_{OH+2,3\text{-DMB}} = 2.287 \times 10^{-17} T^{1.958} \exp(365\ K/T)\ cm^3\ molecule^{-1}\ s^{-1} \quad (220-1292\ K)$$

The experimental data and the evaluations obtained for these five larger alkanes in the present work were used along with prior data/evaluations obtained in this laboratory for H abstractions by OH from a series of smaller alkanes (C_3-C_5) to devise rate rules for abstractions from various types of primary, secondary, and tertiary H atoms. Specifically, the current scheme was applied with good success to H abstractions by OH from a series of *n*-alkanes (*n*-octane through *n*-hexadecane). The total rate constants using this group scheme for reactions of OH with selected large alkanes are given as three-parameter fits in this article. The rate constants for the various abstraction channels in any large *n*-alkane can also be obtained using the groups listed in this article. The present group scheme serves to reduce the uncertainties in rate constants for OH + alkane reactions.

Introduction

Gasoline, diesel, and aviation commercial fuels contain significant amounts of a large number of straight-chain and branched alkanes ($>C_5$). However, natural gas and liquefied petroleum gas (LPG) are almost entirely composed of several smaller ($<C_5$) alkanes. To simplify the chemical complexities in such real-world fuels, there has been significant activity within the combustion community to define surrogates (approximately one or two components representing each chemical class in a real fuel) that can adequately represent, for example, gasoline,[1] diesel,[2] and jet fuels.[3] Large straight-chain alkanes, such as *n*-decane and *n*-hexadecane (cetane), and large branched alkanes, such as 2,2,4-trimethylpentane (*iso*-octane) and 2,2,4,4,6,8,8-heptamethylnonane (*iso*-cetane), are prominent surrogate candidates for the three primary commercial transportation fuels.[1−3] Recent studies have also demonstrated that large *n*-alkanes such as cetane and *n*-decane can be used as surrogates for the combustion of rapeseed oil methyl ester[4] and methyldecanoate,[5] both of which are components of biodiesel.

The reactions studied in this work are H-atom abstractions from alkanes by OH radicals. These are dominant fuel-consumption pathways not only under atmospheric conditions,[6] but also at high temperatures in practical combustion systems that involve oxygen-rich or stoichiometric mixtures.[7] Despite

* Corresponding author. Address: Dr. J. V. Michael, D-193, Bldg. 200, Argonne National Laboratory, Argonne, IL 60439. Phone: (630) 252-3171. Fax: (630) 252-4470. E-mail: jmichael@anl.gov.

10.1021/jp810987u CCC: $40.75
Published on Web 04/06/2009

their importance as primary reactions that govern fuel destruction, a brief survey of the NIST Chemical Kinetics Database[8] indicates a lack of direct experimental rate constant measurements for OH with even smaller *n*- and/or *iso*-alkanes (C_3-C_5) at combustion temperatures above 500 K, with the exceptions being the measurements of Tully and co-workers[9−13] and the single-temperature measurements on a variety of alkanes by Cohen and co-workers.[14−17]

The studies of Tully and co-workers[9−13] were aimed at systematically characterizing the effects of site-specific (primary, secondary, tertiary) H abstractions by utilizing the laser photolysis/laser induced fluorescence (LP-LIF) technique to obtain precise rate constant measurements for OH with a series of small alkanes over a fairly wide temperature range (287−903 K). However, because these rate constants exhibit significant curvature (non-Arrhenius behavior),[18] extrapolating the measurements[9−13] to the higher temperatures found in practical combustion systems requires care. To better quantify the non-Arrhenius behavior, Cohen[18] used a group-additivity transition-state-theory (TST) model that was subsequently tuned[19] to reproduce shock-tube experiments at ∼1200 K for a few selected straight-chain and branched alkanes.[14−16] Athough Cohen's seminal work[19] successfully utilized this group-additivity TST model to make predictions for rate constants over wide temperature ranges for a variety of alkanes, the single-temperature measurements are insufficient to accurately describe the non-Arrhenius behavior at high temperature. Consequently, a primary goal of the present study was to obtain unambiguous direct measurements for the reactions of OH with a series of medium- to large-sized alkanes (C_5-C_8) over wide temperature ranges (800−1300 K) using tBH (*tert*-butyl hydroperoxide) as the OH source. This work completes studies from this laboratory on the reactions of OH with alkanes that were initiated with studies on small to midsized alkanes[20] and cycloalkanes.[21]

The present high-*T* measurements were then used with earlier low-*T* experiments to generate evaluated rate expressions that are valid over wide temperature ranges. These evaluations were then used in conjunction with the evaluations generated for the smaller alkanes in prior work[20] to develop an updated group scheme for specific primary, secondary, and tertiary abstractions using Cohen's[19] group formulation. This updated scheme was then used to make predictions of rate constants for OH reactions with a variety of larger alkanes that are experimentally intractable. In particular, the group scheme was able to make predictions of the rate constants for OH + *n*-alkanes (up to *n*-cetane) with good accuracy (uncertainties <20%) over a wide temperature range (298−2000 K).

Experiments

The present experiments were performed with the reflected-shock-tube technique using OH-radical electronic absorption. The methods and the apparatus have been previously described,[22,23] and only a brief description of the experiments is presented here. The shock tube was fabricated from 304 stainless steel in three sections. The first section, a 10.2-cm-o.d. cylindrical tube, was separated from the He driver chamber by a 4-mil unscored 1100-H18 aluminum diaphragm, and a second 0.25-m transition section then connected the first and third sections. The third section was of rounded-corner (1.71-cm radius) square design and was fabricated from flat stock (3 mm) with a mirror finish. The tube was routinely pumped between experiments to less than 10^{-8} Torr by an Edwards Vacuum Products model CR100P packaged pumping system. Incident shock-wave velocities were measured with eight equally spaced pressure transducers (PCB Piezotronics, Inc., model 113A21) mounted along the third section and recorded with a 4094C Nicolet digital oscilloscope. As described previously, corrections for boundary-layer perturbations have been applied[24−26] for determining both temperature and density in the reflected-shock-wave regime.

For OH detection at 308 nm, a White cell, radially located 6 cm from the end plate (as described previously[27−29]), was used to increase the absorption path length. It was constructed from two flat fused-silica windows (3.81 cm), mounted on the tube across from one another, with a broadband antireflection (BB AR) coating for UV light. The distance between windows was 8.745 cm. The optical configuration consisted of an OH resonance lamp,[27,28] multipass reflectors, an interference filter at 308 nm, and a photomultiplier tube (1P28) all mounted external to the shock tube. The photomultiplier signal was recorded with a LC334A LeCroy digital oscilloscope. At the entrance to the multipass cell, OH resonance radiation was collimated with a set of lenses and was focused onto the reflector on the opposite side of the shock tube through the two AR-coated windows that were flush-mounted to the inside of the shock tube. The reflectors and windows were obtained from CVI Laser Corporation. These reflectors were attached to adjustable mounts, and the center points of windows and mirrors were all in a coaxial position. With this new configuration, 48−58 multiple passes were used, thereby amplifying the measured absorbances by up to ∼4.5 over that used in the previous work.[28,29] This increase in sensitivity for OH-radical detection allows for the detection of lower OH concentration and therefore decreases the importance of secondary reaction perturbations.

Gases. High-purity He (99.995%), used as the driver gas, was obtained from AGA Gases. Research-grade Kr (99.999%), the diluent gas in reactant mixtures, was from Praxair, Inc. The ∼10 ppm impurities (N_2 < 5 ppm, O_2 < 2 ppm, Ar < 1 ppm, CO_2 < 0.5 ppm, H_2 < 1 ppm, H_2O < 3 ppm, Xe < 2 ppm, and total hydrocarbons < 0.2 ppm) were all either inert or in sufficiently low concentration so as to not perturb OH-radical profiles. The microwave-driven OH lamp was operated at 70 W and ∼25 Torr pressure. Distilled water, evaporated at 1 atm into ultra-high-purity-grade Ar (99.999%, from AGA Gases) was used in the resonance lamp. The hydrocarbon reactant molecules, *n*-pentane, *n*-hexane, *n*-heptane, 2,3 dimethyl-butane (2,3-DMB), and 2,2,3,3-tetramethylbutane (2,2,3,3-TMB), were obtained from Sigma-Aldrich. The respective purities of all of these molecules were ≥99.8, ≥99.7, ≥99.8, ≥99.5%, and ≥95%, but they were further purified by bulb-to-bulb distillation, retaining only the middle thirds for mixture preparations. The OH source molecule was *tert*-butyl hydroperoxide (tBH). tBH was obtained from Sigma-Aldrich as a water solution (T-HYDRO tBH, ∼70% tBH by weight; i.e., ∼32 mol % tBH and 68 mol % H_2O) and was used as the OH-radical source for the OH + hydrocarbon reaction studies as described previously.[20,30] The gas mixtures were accurately prepared from pressure measurements using a Baratron capacitance manometer and were stored in 22-L glass bulbs in an all-glass vacuum line. The details of the mixture mole fractions used in the present experiments are available in Tables 1−5.

Results

New High-*T* Rate Constants. Figure 1 shows three typical OH concentration profiles measured with *n*-heptane (C_7H_{16}) as the reactant over the available temperature range using tBH as the OH source. tBH dissociation becomes too slow at ∼800−850 K, and for reflected-shock temperatures of ∼1300−1350 K,

TABLE 1: High-*T* Rate Data: OH + *n*-C_7H_{16} → Products

P_1 (Torr)	M_s[a]	ρ_5[b] (10^{18} cm^{-3})	T_5[b] (K)	k_{12}[c]	k_{12}[d]	Φ[e]
		$X_{C_7H_{16}} = 4.578 \times 10^{-5}$, $X_{tBH\ soln} = 2.771 \times 10^{-5}$				
10.86	2.229	1.867	1253	5.20×10^{-11}	5.52×10^{-11}	0.310
10.85	2.120	1.756	1145	4.31×10^{-11}	4.60×10^{-11}	0.310
10.92	2.198	1.853	1218	5.24×10^{-11}	5.43×10^{-11}	0.295
10.89	2.191	1.840	1210	4.74×10^{-11}	5.10×10^{-11}	0.300
10.94	2.147	1.804	1167	4.38×10^{-11}	4.45×10^{-11}	0.360
10.87	2.103	1.747	1125	4.33×10^{-11}	4.45×10^{-11}	0.290
		$X_{C_7H_{16}} = 4.578 \times 10^{-5}$, $X_{tBH\ soln} = 2.771 \times 10^{-5}$				
15.82	1.891	2.221	942	3.10×10^{-11}	2.95×10^{-11}	0.400
15.82	1.991	2.382	1031	3.97×10^{-11}	4.10×10^{-11}	0.340
15.88	2.076	2.520	1108	4.07×10^{-11}	4.15×10^{-11}	0.335
15.91	2.088	2.543	1119	4.04×10^{-11}	4.35×10^{-11}	0.330
15.92	2.104	2.568	1134	4.78×10^{-11}	4.65×10^{-11}	0.340
15.92	2.138	2.617	1166	4.36×10^{-11}	4.60×10^{-11}	0.340
15.93	2.206	2.715	1232	4.65×10^{-11}	4.90×10^{-11}	0.330
15.83	2.231	2.732	1257	5.27×10^{-11}	5.55×10^{-11}	0.300
15.89	2.261	2.782	1287	5.05×10^{-11}	5.60×10^{-11}	0.270
15.89	1.934	2.309	977	3.30×10^{-11}	3.40×10^{-11}	0.300
15.95	1.992	2.402	1031	3.59×10^{-11}	3.80×10^{-11}	0.310
		$X_{C_7H_{16}} = 2.744 \times 10^{-5}$, $X_{tBH\ soln} = 1.260 \times 10^{-5}$				
30.65	1.798	3.904	846	2.76×10^{-11}	2.40×10^{-11}	0.370
30.86	1.777	3.822	838	2.93×10^{-11}	2.60×10^{-11}	0.350
30.73	1.818	3.928	875	2.96×10^{-11}	2.75×10^{-11}	0.360
30.99	1.842	4.038	895	3.34×10^{-11}	3.00×10^{-11}	0.350
30.65	1.866	4.071	915	3.38×10^{-11}	3.10×10^{-11}	0.370
30.68	1.883	4.099	935	3.38×10^{-11}	3.25×10^{-11}	0.370

[a] Error in measuring the Mach number, M_s, is typically 0.5−1.0% at the level of one standard deviation. [b] Quantities with the subscript 5 refer to the thermodynamic state of the gas in the reflected shock region. [c] Pseudo-first-order rate constants in units of cm^3 molecule^{-1} s^{-1}. [d] Rate constants from modeling OH profiles using a 49-reaction, 29-species mechanism in units of cm^3 molecule^{-1} s^{-1}. [e] $\Phi = X_{tBH}/X_{tBH\ soln}$.

TABLE 2: High-*T* Rate Data: OH + 2,2,3,3-TMB → *neo*-C_8H_{17} + OH

P_1 (Torr)	M_s[a]	ρ_5[b] (10^{18} cm^{-3})	T_5[b] (K)	k_{12}[c]	k_{12}[d]	Φ[e]
		$X_{C_8H_{18}} = 4.229 \times 10^{-5}$, $X_{tBH\ soln} = 2.639 \times 10^{-5}$				
15.94	1.805	2.058	885	1.93×10^{-11}	1.93×10^{-11}	0.300
15.93	2.005	2.379	1061	2.28×10^{-11}	2.35×10^{-11}	0.300
15.98	1.956	2.310	1016	2.26×10^{-11}	2.20×10^{-11}	0.320
15.98	1.883	2.185	955	2.07×10^{-11}	2.05×10^{-11}	0.315
15.94	1.901	2.217	967	2.25×10^{-11}	2.14×10^{-11}	0.320
15.84	1.883	2.167	955	2.07×10^{-11}	2.00×10^{-11}	0.315
15.94	1.860	2.151	933	2.04×10^{-11}	1.94×10^{-11}	0.330
15.86	1.849	2.121	923	2.05×10^{-11}	1.90×10^{-11}	0.310
15.94	1.829	2.091	909	1.99×10^{-11}	1.85×10^{-11}	0.320
		$X_{C_8H_{18}} = 4.229 \times 10^{-5}$, $X_{tBH\ soln} = 2.639 \times 10^{-5}$				
30.79	1.707	3.540	789	1.36×10^{-11}	1.49×10^{-11}	0.300
30.91	1.766	3.755	837	1.73×10^{-11}	1.70×10^{-11}	0.316

[a] Error in measuring the Mach number, M_s, is typically 0.5−1.0% at the level of one standard deviation. [b] Quantities with the subscript 5 refer to the thermodynamic state of the gas in the reflected shock region. [c] Pseudo-first-order rate constants in units of cm^3 molecule^{-1} s^{-1}. [d] Rate constants from modeling OH profiles using a 46-reaction, 27-species mechanism in units of cm^3 molecule^{-1} s^{-1}. [e] $\Phi = X_{tBH}/X_{tBH\ soln}$.

dissociation in the incident shock regime occurs, thus complicating the analysis. The solid lines shown in the figure are fits using our 49-reaction, 29-species mechanism,[20] with fits to $k_{OH+C_7H_{16}}$ included as the main loss process for OH. A few reactions were also added to reflect possible perturbing reactions that might be specific to heptane (e.g., C_7H_{16} decomposition followed by OH reactions with subsequent products). For the initial tBH concentration ($[tBH]_0$) used in the present study, secondary reactions were found to be of minor importance, as shown in the linear sensitivity analysis of Figure 2 for the highest-*T* experiment (1210 K) of Figure 1. The main perturbing reactions are OH + acetone and OH + CH_3, showing small effects but only at long times. The extent of perturbation is even less in the lower-*T* experiments of Figure 1. However, the choices of rate constants for $k_{OH+C_7H_{16}}$ are quite sensitive as seen, for example, in Figure 1, where ±20% simulations from the best fit for the results shown in Figure 1 are included as bold dashed lines.

As starting values in full mechanistic simulations, we first estimated $k_{OH+C_7H_{16}}$ from pseudo-first-order analyses for the long-time profiles as $k_{first}/[C_7H_{16}]_0$, where k_{first} is the measured apparent first-order decay constant and $[C_7H_{16}]_0$ is the initial concentration of *n*-heptane. We found that the first-order analytical method gave long-time profiles that were, within experimental error, always in agreement with experiment; however, some slight individual adjustments were made in the final simulations. In general, the results from strictly first-order analysis and complete profile simulations were within ±7%, reiterating the conclusion that secondary reactions are not important in this case. Nevertheless, the complete simulation results for $k_{OH+C_7H_{16}}$ are listed in Table 1. From these simulations, the initial concentration of tBH necessary to reproduce the

TABLE 3: High-*T* Rate Data: OH + *n*-C_5H_{12} → Products

P_1 (Torr)	M_s[a]	ρ_5[b] (10^{18} cm^{-3})	T_5[b] (K)	k_{12}[c]
$X_{C_5H_{12}} = 8.802 \times 10^{-5}$, $X_{tBH\ soln} = 2.749 \times 10^{-5}$				
10.98	2.284	1.942	1308	4.21×10^{-11}
10.95	2.281	1.934	1305	3.82×10^{-11}
10.85	2.178	1.810	1205	3.50×10^{-11}
10.90	2.173	1.819	1196	3.17×10^{-11}
10.91	2.174	1.822	1197	3.06×10^{-11}
10.89	2.188	1.839	1207	3.42×10^{-11}
10.86	2.207	1.853	1225	3.44×10^{-11}
$X_{C_5H_{12}} = 8.802 \times 10^{-5}$, $X_{tBH\ soln} = 2.749 \times 10^{-5}$				
15.85	2.186	2.666	1216	3.22×10^{-11}
15.90	2.126	2.590	1159	2.60×10^{-11}
15.99	2.038	2.473	1076	2.61×10^{-11}
15.86	1.933	2.289	982	2.23×10^{-11}
15.96	1.834	2.274	897	1.93×10^{-11}
15.91	1.764	2.012	839	1.91×10^{-11}
15.92	1.881	2.220	934	2.28×10^{-11}
15.87	1.934	2.292	983	2.15×10^{-11}
15.99	2.070	2.530	1102	2.93×10^{-11}
15.92	1.745	1.979	823	1.31×10^{-11}
15.88	1.876	2.198	932	2.20×10^{-11}
$X_{C_5H_{12}} = 4.410 \times 10^{-5}$, $X_{tBH\ soln} = 1.237 \times 10^{-5}$				
30.63	1.803	3.919	850	1.92×10^{-11}
30.82	1.883	4.205	917	1.76×10^{-11}
30.69	1.947	4.388	972	2.74×10^{-11}
30.88	1.905	4.281	935	1.97×10^{-11}
30.86	1.947	4.412	972	2.05×10^{-11}
30.79	1.975	4.488	996	2.63×10^{-11}
30.64	2.043	4.669	1057	2.77×10^{-11}
30.69	2.045	4.680	1058	2.49×10^{-11}

[a] Error in measuring the Mach number, M_s, is typically 0.5−1.0% at the level of one standard deviation. [b] Quantities with the subscript 5 refer to the thermodynamic state of the gas in the reflected shock region. [c] Pseudo-first-order rate constants in units of cm^3 molecule^{-1} s^{-1}.

TABLE 4: High-*T* Rate Data: OH + *n*-C_6H_{14} → Products

P_1 (Torr)	M_s[a]	ρ_5[b] (10^{18} cm^{-3})	T_5[b] (K)	k_{12}[c]
$X_{C_6H_{14}} = 1.075 \times 10^{-4}$, $X_{tBH\ soln} = 2.537 \times 10^{-5}$				
10.98	2.081	1.742	1103	3.52×10^{-11}
10.93	2.099	1.748	1124	4.12×10^{-11}
10.93	2.092	1.740	1117	3.28×10^{-11}
10.97	2.176	1.834	1199	3.64×10^{-11}
10.93	2.276	1.925	1299	5.66×10^{-11}
10.88	2.224	1.867	1247	4.58×10^{-11}
10.89	2.213	1.858	1236	4.50×10^{-11}
10.92	2.169	1.818	1191	3.73×10^{-11}
10.92	2.100	1.747	1125	3.17×10^{-11}
10.96	2.135	1.790	1159	3.70×10^{-11}
10.92	2.170	1.819	1193	4.05×10^{-11}
$X_{C_6H_{14}} = 1.075 \times 10^{-4}$, $X_{tBH\ soln} = 2.537 \times 10^{-5}$				
15.96	1.959	2.361	998	2.82×10^{-11}
15.92	1.955	2.349	994	3.05×10^{-11}
15.93	1.879	2.226	929	2.57×10^{-11}
15.85	1.883	2.221	932	2.39×10^{-11}
15.86	1.816	2.109	876	2.14×10^{-11}
15.86	2.021	2.436	1057	2.92×10^{-11}
$X_{C_6H_{14}} = 5.477 \times 10^{-5}$, $X_{tBH\ soln} = 1.248 \times 10^{-5}$				
30.84	1.963	4.428	992	2.56×10^{-11}
30.99	1.872	4.162	913	2.09×10^{-11}
30.94	1.859	4.128	899	2.20×10^{-11}
30.70	1.828	3.996	873	2.04×10^{-11}
30.89	1.735	3.710	798	1.51×10^{-11}

[a] Error in measuring the Mach number, M_s, is typically 0.5−1.0% at the level of one standard deviation. [b] Quantities with the subscript 5 refer to the thermodynamic state of the gas in the reflected shock region. [c] Pseudo-first-order rate constants in units of cm^3 molecule^{-1} s^{-1}.

maxima (see Figure 1) turned out to be (33 ± 3) mol % of the T-HYDRO tBH solution, in agreement with the assay provided by Sigma-Aldrich. An Arrhenius plot of the data for OH + heptane from Table 1 is shown in Figure 3.

The conditions for the experiments with 2,2,3,3-TMB are given in Table 2. Because the ratio of initial concentrations, $[C_8H_{18}]_0/[tBH]_0$, was relatively small (as with the OH + *n*-C_7H_{16} experiments), the presumption of first-order behavior is questionable. Hence, all experiments were simulated, with a 46-reaction, 27-species mechanism including reactions of the thermal decomposition of 2,2,3,3-TMB and its subsequent products with OH. Because there is significant thermal decomposition of 2,2,3,3-tetramethylbutane at $T > 1100$ K, we restricted our experiments to a lower T range, 789−1061 K, to avoid interferences from secondary reactions (that is, reactions of OH with the thermal decomposition products). Figure 4 shows a typical profile, with Figure 5 being a linear sensitivity analysis of the experiment. As before, the initial value for $k_{OH+C_8H_{18}}$ was determined from pseudo-first-order analysis, and these values were further modified to obtain a best fit to the profile. The results for $k_{OH+C_8H_{18}}$ are given in Table 2, and the initial concentration of tBH necessary to reproduce the maxima for the set is (31.5 ± 1.0) mol %, in agreement with the assay provided by Sigma-Aldrich. An Arrhenius plot of the data for OH + 2,2,3,3-TMB from Table 2 is shown in Figure 6.

The rate constants for the other three molecules, *n*-pentane, *n*-hexane, and 2,3-DMB, could be analyzed using the pseudo-first-order method (i.e., $k_{OH+alkane} = k_{first}/[alkane]_0$) because the alkane-to-tBH ratios were substantially higher than for *n*-heptane and *neo*-octane. Hence, the reactions were essentially chemically isolated. The bimolecular rate constants are listed in Tables 3−5, and Arrhenius plots are shown in Figures 7−9.

The data for OH + *n*-pentane (Table 3) are the first determinations at $T > 800$ K; however, Bott and Cohen[16] measured one value at 1220 K for OH + 2,3-DMB and one value at 1180 K for OH + 2,2,3,3-TMB. For the two other alkanes studied in this work, OH + *n*-hexane and OH + *n*-heptane, the only high-T measurements (>500 K) are those of Koffend and Cohen[17] at 962 and 1186 K, respectively.

Arrhenius plots of the rate constants from Tables 1−5 are shown in Figures 3 and 6−9, and, in units of cm^3 molecule^{-1} s^{-1}, these data can be represented as

$$k_{OH+n\text{-heptane}} = (2.48 \pm 0.17) \times 10^{-10} \exp[(-1927 \pm 69\ \text{K})/T] \quad (838-1287\ \text{K}) \quad (1)$$

$$k_{OH+2,2,3,3\text{-TMB}} = (8.26 \pm 0.89) \times 10^{-11} \exp[(-1337 \pm 94\ \text{K})/T] \quad (789-1061\ \text{K}) \quad (2)$$

$$k_{OH+n\text{-pentane}} = (1.60 \pm 0.25) \times 10^{-10} \exp[(-1903 \pm 146\ \text{K})/T] \quad (823-1308\ \text{K}) \quad (3)$$

$$k_{OH+n\text{-hexane}} = (2.79 \pm 0.39) \times 10^{-10} \exp[(-2301 \pm 134\ \text{K})/T] \quad (798-1299\ \text{K}) \quad (4)$$

$$k_{OH+2,3\text{-DMB}} = (1.27 \pm 0.16) \times 10^{-10} \exp[(-1617 \pm 118\ \text{K})/T] \quad (843-1292\ \text{K}) \quad (5)$$

over the indicated temperature ranges. In all cases, the experimental data are within ±18% of the lines determined by eqs 1−5.

Extended-Temperature-Range Evaluations. A substantial experimental database, obtained at lower temperatures, exists

TABLE 5: High-*T* Rate Data: OH + 2,3-DMB → Products

P_1 (Torr)	M_s[a]	ρ_5[b] (10^{18} cm^{-3})	T_5[b] (K)	k_{12}[c]
$X_{2,3\text{-DMB}} = 7.220 \times 10^{-5}$, $X_{\text{tBH soln}} = 2.461 \times 10^{-5}$				
10.79	2.251	1.851	1292	4.01×10^{-11}
10.86	2.207	1.821	1247	3.72×10^{-11}
10.85	2.166	1.778	1206	3.50×10^{-11}
10.90	2.121	1.741	1161	3.10×10^{-11}
10.84	2.065	1.674	1107	2.98×10^{-11}
10.86	2.143	1.757	1183	3.17×10^{-11}
10.86	2.187	1.795	1231	3.35×10^{-11}
10.89	2.209	1.828	1249	3.94×10^{-11}
$X_{2,3\text{-DMB}} = 7.220 \times 10^{-5}$, $X_{\text{tBH soln}} = 2.461 \times 10^{-5}$				
15.82	1.818	2.071	893	2.13×10^{-11}
15.79	1.989	2.343	1043	2.75×10^{-11}
15.83	2.032	2.414	1082	2.69×10^{-11}
15.79	2.098	2.504	1144	2.76×10^{-11}
15.88	2.107	2.523	1156	3.07×10^{-11}
15.90	1.984	2.351	1038	2.39×10^{-11}
15.96	1.985	2.362	1039	2.40×10^{-11}
15.86	1.952	2.294	1009	2.46×10^{-11}
15.88	1.912	2.226	977	2.27×10^{-11}
$X_{2,3\text{-DMB}} = 4.086 \times 10^{-5}$, $X_{\text{tBH soln}} = 1.239 \times 10^{-5}$				
30.82	1.777	3.791	843	2.13×10^{-11}
30.94	1.830	3.979	887	1.97×10^{-11}
30.74	1.812	3.896	872	2.19×10^{-11}
30.88	1.889	4.159	938	2.45×10^{-11}
30.90	1.897	4.159	951	2.24×10^{-11}
30.86	1.888	4.153	937	2.09×10^{-11}
30.94	1.830	3.979	887	1.94×10^{-11}
30.68	1.808	3.875	869	2.07×10^{-11}

[a] Error in measuring the Mach number, M_s, is typically 0.5−1.0% at the level of one standard deviation. [b] Quantities with the subscript 5 refer to the thermodynamic state of the gas in the reflected shock region. [c] Pseudo-first-order rate constants in units of cm^3 molecule^{-1} s^{-1}.

for the reactions studied in this work, with the bulk of the studies being room-temperature measurements as summarized in the NIST database.[8] Specifically, for the OH + *n*-heptane reaction, seven measurements and several evaluations are listed. In the present evaluation, we chose only the seven measurements along with the present high-*T* measurements. Along with our high-*T* data, the evaluation includes the measurements of Koffend and Cohen[17] (1186 K), Ferrari et al.[31] (295 K), Anderson et al.[32] (295 K), Wilson et al.[33] (241−406 K), Anderson et al.[34] (296 K), Atkinson et al.[35] (299 K), and Klopffer et al.[36] (300 K). Five equally spaced points in T^{-1} were determined from reported Arrhenius expressions, but only over the *T* range of a given study. These (along with the points at a single temperature) comprise a database of experimental rate constants that spans a wide temperature range (241−1287 K). Including the present work, each temperature-dependent study, therefore, was given equal statistical weight. The resultant 16 points from the eight OH + *n*-heptane studies (six studies were single-*T* values) were then fitted to a three-parameter expression of the form $k = AT^n \exp(-B/T)$, giving

$$k_{\text{OH+}n\text{-heptane}} = 2.059 \times 10^{-15} T^{1.401} \exp(33\ \text{K}/T)\ \text{cm}^3\ \text{molecule}^{-1}\ \text{s}^{-1} \quad (241-1287\ \text{K}) \quad (6)$$

Equation 6 is within ±16% of the lowest-*T* (241 K) and highest-*T* (1287 K) data points. Koffend and Cohen's[17] 1186 K measurement is 22% lower than eq 6, and the Klopffer et al.[36] room-*T* measurement exhibits the largest deviation, being 25% higher than eq 6.

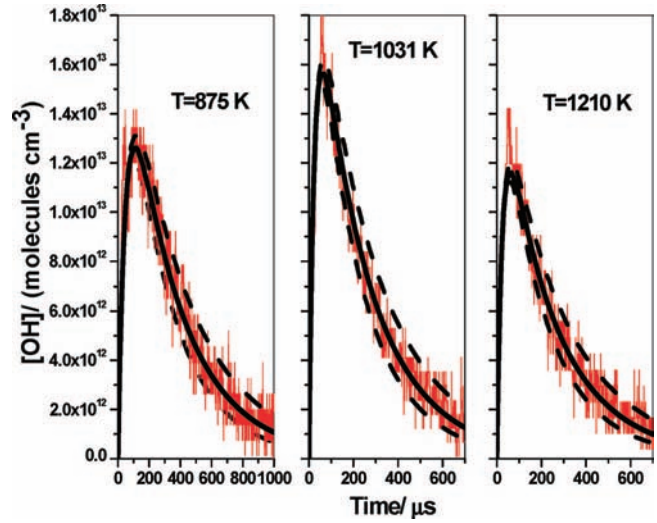

Figure 1. Three OH concentration profiles at 875, 1031, and 1210 K from the OH + *n*-C_7H_{16} data set. The solid lines are fits over the entire time range using a 49-step, 29-species reaction mechanism with k_1 obtained from pseudo-first-order analyses. The dashed lines are fits with changes in k_1 by ±20%. The conditions for the experiment at T_5 = 875 K were P_1 = 30.73 Torr, M_s = 1.818, $\rho_5 = 3.928 \times 10^{18}$ molecules cm^{-3}, $[\text{tBH}]_0 = 1.592 \times 10^{13}$ molecules cm^{-3}, $[\text{H}_2\text{O}]_0 = 2.830 \times 10^{13}$ molecules cm^{-3}, and $[n\text{-C}_7\text{H}_{16}]_0 = 1.078 \times 10^{14}$ molecules cm^{-3}. The conditions for the experiment at T_5 = 1031 K were P_1 = 15.82 Torr, M_s = 1.991, $\rho_5 = 2.382 \times 10^{18}$ molecules cm^{-3}, $[\text{tBH}]_0 = 2.244 \times 10^{13}$ molecules cm^{-3}, $[\text{H}_2\text{O}]_0 = 4.355 \times 10^{13}$ molecules cm^{-3}, and $[n\text{-C}_7\text{H}_{16}]_0 = 1.090 \times 10^{14}$ molecules cm^{-3}. The conditions for the experiment at T_5 = 1210 K were P_1 = 10.89 Torr, M_s = 2.191, $\rho_5 = 1.840 \times 10^{18}$ molecules cm^{-3}, $[\text{tBH}]_0 = 1.530 \times 10^{13}$ molecules cm^{-3}, $[\text{H}_2\text{O}]_0 = 3.569 \times 10^{13}$ molecules cm^{-3}, and $[n\text{-C}_7\text{H}_{16}]_0 = 8.426 \times 10^{13}$ molecules cm^{-3}.

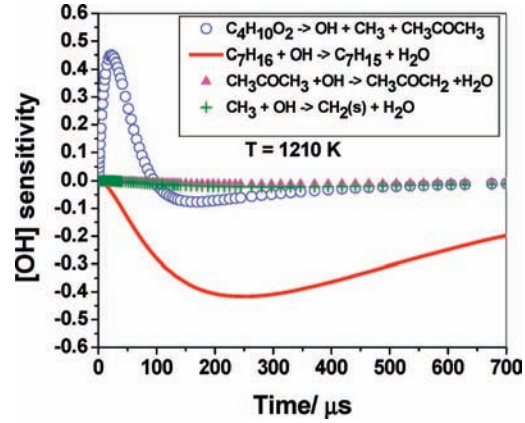

Figure 2. OH-radical sensitivity analysis for the 1210 K profile shown in Figure 1 using the full reaction mechanism and the modeled rate constants in Table 1. The four most sensitive reactions are shown in the inset.

Using the same procedure, experimental evaluations were generated for the four other alkanes studied in this work. For OH + 2,2,3,3-TMB, the present evaluation included the measurements of Tully et al.[9] (290−737.5 K), Greiner[37] (294−495 K), Atkinson et al.[38] (299 K), Bott and Cohen[16] (1180 K), and the present high-*T* results. As before, five equally spaced points in T^{-1} were determined from reported Arrhenius expressions, but only over the *T* range of a given study. This procedure generated a database of experimental rate constants that spans a wide *T* range (290−1180 K). The resultant 17 points from the five OH + 2,2,3,3-TMB studies (two studies were single-*T* values) were then fitted to a three-parameter expression, giving

$$k_{\mathrm{OH+2,2,3,3\text{-}TMB}} = 6.835\times10^{-17}T^{1.886}\exp(-365\ \mathrm{K}/T)\ \mathrm{cm^3\ molecule^{-1}\ s^{-1}} \quad (290-1180\ \mathrm{K})\ (7)$$

Equation 7 provides an excellent fit to the five data sets, being <21% lower than the lowest-T value (789 K) from the present experiments.

For OH + n-pentane, the present evaluation included our high-T measurements (the only available data at T > 800 K) and the measurements of DeMore and Bayes[39] (233−364 K), Donahue and Anderson[40] (300−390 K), Talukdar et al.[41] (224−372 K), Iannone et al.[42] (298 K), Abbatt et al.[43] (297 K), Nolting et al.[44] (312 K), Atkinson et al.[35] (299 K), Cox et al.[45] (298 K), and Darnall et al.[46] (300 K). Consequently, the 26 points from these 10 OH + n-pentane data sources (six studies were single-T values) were fitted as before to a three-parameter expression, giving

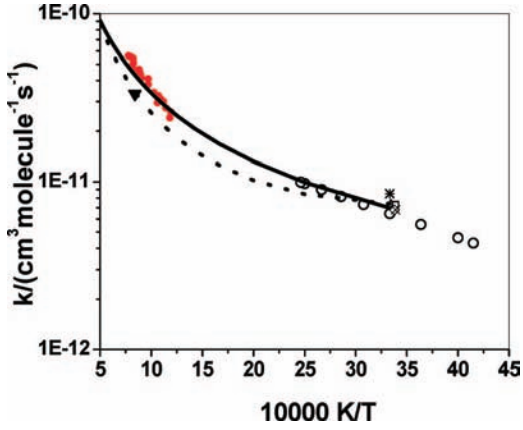

Figure 3. Arrhenius plot of the OH + n-C_7H_{16} rate constants. (●) Experiments, present work, 838−1287 K; (—) three-parameter fit to groups, present work, 298−2000 K, eq 19; (• • •) Cohen,[19] TST total rate, 298−2000 K; (▼) Koffend and Cohen,[17] 1190 K; (Δ) Atkinson et al.,[35] 299 K; (◊) Anderson et al.,[34] 296 K; (*) Klopffer et al.,[36] 300 K; (○) Wilson et al.,[33] 241−406 K; (□) Ferrari et al.,[31] 295 K; (×) Anderson et al.,[32] 295 K.

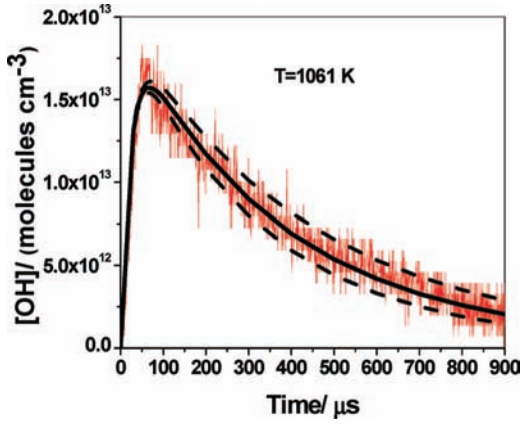

Figure 4. OH concentration profile at 1061 K from the OH + 2,2,3,3-TMB data set. The solid line is a fit over the entire time range using a 46-step, 27-species reaction mechanism with k_1 obtained from pseudo-first-order analyses. The dashed lines are fits with changes in k_1 by ±20%. The conditions for the experiment at T_5 = 1061 K were P_1 = 15.93 Torr, M_s = 2.005, $\rho_5 = 2.379\times10^{18}$ molecules cm^{-3}, $[\mathrm{tBH}]_0 = 1.884\times10^{13}$ molecules cm^{-3}, $[\mathrm{H_2O}]_0 = 4.396\times10^{13}$ molecules cm^{-3}, and $[2,2,3,3\text{-TMB}]_0 = 1.006\times10^{14}$ molecules cm^{-3}.

$$k_{\mathrm{OH+}n\text{-pentane}} = 2.495\times10^{-16}T^{1.649}\exp(80\ \mathrm{K}/T)\ \mathrm{cm^3\ molecule^{-1}\ s^{-1}} \quad (224-1308\ \mathrm{K})\ (8)$$

Equation 8 provides an excellent fit to the high-T data, being within 10% over the present T range. The Cox et al.[45] room-T measurement is 28% higher with the other room- and lower-temperature (<500 K) measurements, being within ±17% of eq 8.

For OH + n-hexane the present evaluation included our high-T measurements (798−1299 K), the single-point measurement of Koffend and Cohen[17] (962 K), and the lower-T measurements of DeMore and Bayes[39] (292−367 K), Donahue and Anderson[40] (300−390 K), Anderson et al.[34] (296 K), McLoughlin et al.[47] (301 K), Nolting et al.[44] (312 K), Atkinson et al.[35] (299 K), Atkinson et al.[38] (295 K), Klopffer et al.[36] (300 K), Barnes et al.[48] (300 K), Lloyd et al.[49] (305 K), and Campbell et al.[50] (292 K). The 25 points from these 13 OH + n-hexane data sources (10 studies were single-T values) were fitted as before to a three-parameter expression, giving

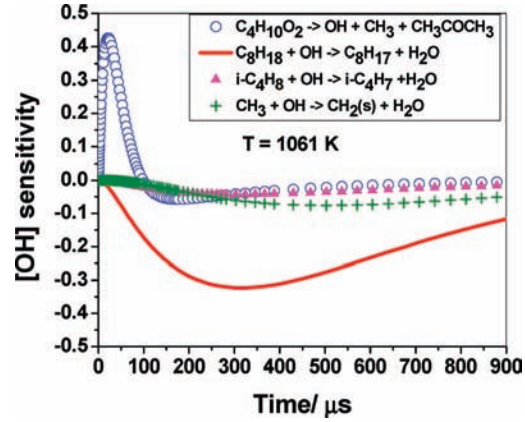

Figure 5. OH-radical sensitivity analysis for the 1061 K profile shown in Figure 1 using the full reaction mechanism and the modeled rate constants in Table 2. The four most sensitive reactions are shown in the inset.

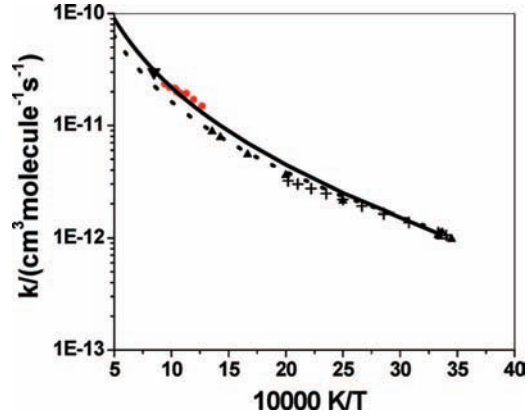

Figure 6. Arrhenius plot of the OH + 2,2,3,3-TMB rate constants. (●) Experiments, present work, 789−1061 K; (—) three-parameter fit to groups, present work, 298−2000 K, eq 41; (• • •) Cohen,[19] TST total rate, 298−2000 K; (▲) Tully et al.,[9] 290−737.5 K; (+) Greiner,[37] 294−495 K; (▼) Bott and Cohen,[16] 1180 K; (Δ) Atkinson et al.,[38] 297 K.

$$k_{\mathrm{OH}+n\text{-hexane}} = 3.959\times10^{-18}T^{2.218}\exp(443\ \mathrm{K}/T)\ \mathrm{cm}^3\ \mathrm{molecule}^{-1}\ \mathrm{s}^{-1} \quad (292-1299\ \mathrm{K})\ (9)$$

The Anderson et al.[32] 295 K measurement appears to be an outlier with respect to the other room-temperature measurements, being ~70% lower than the average value reported at room temperature. The Anderson et al.[32] value was therefore not used in generating the evaluation. Equation 9 again provides an excellent fit to the present high-T data, being within ±25% of the data sets chosen for the evaluation.

Finally, the NIST database[8] lists seven direct measurements for the OH + 2,3-DMB rate constant, with the Bott and Cohen[16] measurement being the only one at high T (>500 K). The present evaluation included our high-T experiments (843−1292 K) along with the single-point measurement of Bott and Cohen[16] (1220 K) and the lower-T studies by Wilson et al.[33] (220−407 K), Atkinson et al.[35] (299 K), Cox et al.[45] (298 K), Darnall et al.[46] (300 K), and Darnall et al.[51] (305 K). Greiner's[37] measurements showed rate constants decreasing with increasing temperatures, a trend not observed in other experiments, and therefore, they were not used in the experimental evaluation. The 15 points from the seven OH + 2,3-DMB data sources (five studies were single-T values) were fitted as before to a three-parameter expression, giving

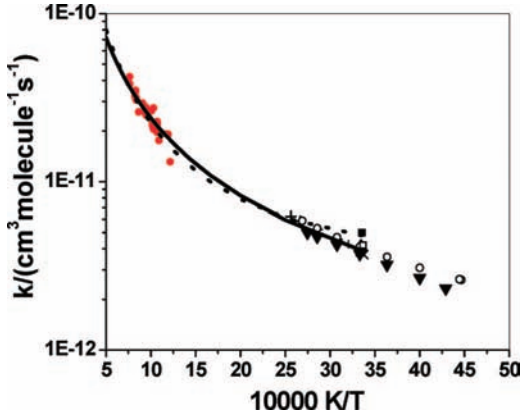

Figure 7. Arrhenius plot of the OH + n-C_5H_{12} rate constants. (●) Experiments, present work, 823−1308 K, (—) three-parameter fit to groups, present work, 298−2000 K, eq 8; (• • •) Cohen,[19] TST total rate, 298−2000 K; (♦) DeMore and Bayes,[39] 233−364 K; (+) Donahue et al.,[40] 300−390 K; (○) Talukdar et al.,[41] 224−372 K; (×) Iannone et al.,[42] 298 K; (□) Abbatt et al.,[43] 297 K; (|) Nolting et al.,[44] 312 K; (■) Cox et al.,[45] 298 K; (Δ) Atkinson et al.,[35] 299 K; (▲) Darnall et al.,[46] 300 K.

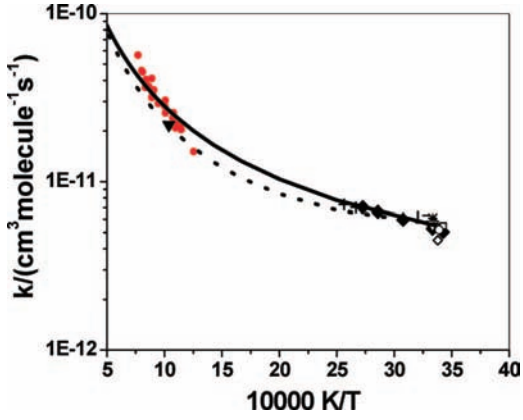

Figure 8. Arrhenius plot of the OH + n-C_6H_{14} rate constants. (●) Experiments, present work, 798−1299 K; (—) three-parameter fit to groups, present work, 298−2000 K, eq 16; (• • •) Cohen,[19] TST total rate, 298−2000 K; (▼) Koffend and Cohen,[17] 962 K; (♦) DeMore and Bayes,[39] 292−367 K; (+) Donahue et al.,[40] 300−390 K; (◊) Anderson et al.,[34] 296 K; (■) McLoughlin et al.,[47] 301 K; (○) Atkinson et al.,[38] 295 K; (*) Klopffer et al.,[36] 300 K; (▽) Barnes et al.,[48] 300 K; (—) Lloyd et al.,[49] 305 K; (|) Nolting et al.,[44] 312 K; (□) Campbell et al.,[50] 292 K; (Δ) Atkinson et al.,[35] 299 K.

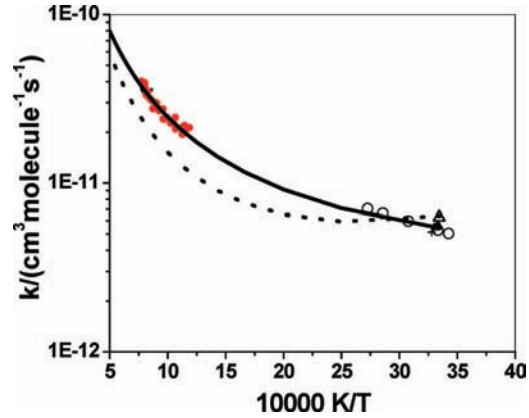

Figure 9. Arrhenius plot of the OH + 2,3-DMB rate constants. (●) Experiments, present work, 843−1292 K; (—) three-parameter fit to groups, present work, 298−2000 K, eq 10; (• • •) Cohen,[19] TST total rate, 298−2000 K; (▼) Bott and Cohen,[16] 1220 K; (○) Wilson et al.,[33] 220−407 K; (Δ) Atkinson et al.,[35] 299 K; (■) Cox et al.,[45] 298 K; (▲) Darnall et al.,[46] 300 K; (+) Darnall et al.,[51] 305 K.

$$k_{\mathrm{OH}+2,3\text{-DMB}} = 2.287\times10^{-17}T^{1.958}\exp(365\ \mathrm{K}/T)\ \mathrm{cm}^3\ \mathrm{molecule}^{-1}\ \mathrm{s}^{-1} \quad (220-1292\ \mathrm{K})\ (10)$$

Equation 10 also provides an excellent fit to the high-T (>500 K) data, being within 3% of the present experiments and Bott and Cohen's 1220 K point. The room-temperature measurement of Cox et al.[45] shows the largest deviation, being 30% lower than eq 10.

Discussion

Prior Work. Benson and co-workers[52] pioneered the application of the principle of additivity of bond properties to the interpretation of kinetic data. A number of studies have been moderately successful in developing generic models for predicting rate constants for H abstractions by OH from alkanes. In early studies, Greiner,[37] utilizing his experimental data, proposed a simple additivity model that would be applicable for any alkane. That scheme[37] assumed that all primary, secondary, and tertiary H atoms undergoing abstraction by OH were equivalent. In subsequent work by Baldwin and Walker,[53] a similar scheme (assuming equivalency of various kinds of primary, secondary, and tertiary H atoms) was proposed for predicting rates of OH reactions with any alkane relative to the rate of OH + H_2 → H_2O + H. Atkinson et al.[38] progressed further toward developing a general model by separating the contributions of OH abstractions for different types of secondary and tertiary H atoms that depended on the degree of branching in the alkane. On the basis of the available literature data, Cohen's[19] revised TST model for OH + alkanes argued that there were distinctions between the various kinds of primary and secondary H atoms, but differences among various tertiary H atoms were barely discernible because of the lack of accurate experimental data. His TST-based model provided a theoretical framework for predicting rate constants for abstraction by OH from various primary, secondary, and tertiary H atoms over a wide T range. In recent

work, Huynh et al.[54] adopted a different approach. They correlated rate constants for any general OH + alkane reaction to that for the reference reaction OH + $C_2H_6 \rightarrow H_2O + C_2H_5$, using TST calculations that incorporated reaction class factors and barrier heights derived through linear energy relationships.

In the present work, a substantially different approach has been taken to generalize rate constants for OH + alkane reactions. In our recent experimental and theoretical study on OH + small alkanes,[20] we used high-level ab initio calculations for the energetics, along with conventional transition state theory (CTST) for the prediction of rate constants. The theoretical results were in excellent agreement with the total rate constants measured by a number of investigators (including high-*T* data from this laboratory) over a wide temperature range. The predicted theoretical branching ratios for primary, secondary, and tertiary abstractions in these simple alkanes were in good agreement with the measurements of Tully and co-workers.[9−13] However, it is impractical at the present time to perform high-level ab initio calculations for the reactions of OH with larger ($>C_6$) alkanes. Consequently, we have chosen to apply Cohen's methodology[19] to the available experimental literature database on reactions of OH with a set of C_3-C_8 alkanes in order to extract rates per H atom for individual primary, secondary, and tertiary groups.

A large experimental database on a wide variety of alkanes (up to C_{10}) would be necessary for extracting all possible groups using Cohen's[19] formalism. This procedure is impractical and experimentally difficult for the larger alkanes. As an example, for a C_7 alkane, there are 9 isomers, and as size increases, the number of possible isomers increases to 18 for a C_8 alkane, 35 for a C_9 alkane, and 75 for a C_{10} alkane. However, it will be shown here that experiments on *n*-alkanes (from *n*-pentane through *n*-heptane, coupled with our prior work[20] on propane and *n*-butane) are sufficient to extract the groups required for predicting OH + any larger *n*-alkane. The studies on these *n*-alkanes coupled with studies on *iso*-alkanes and *neo*-alkanes from the present and earlier work[20] can be used to obtain all possible primary abstraction groups and a few targeted secondary and tertiary abstraction groups.

Groups. Using thermochemical arguments, Cohen's[19] TST model was based on defining C—H bonds in alkanes according to next-nearest-neighbor (NNN) configurations. His classification defined primary C—H bonds (in alkanes other than methane) as P_0 (ethane), P_1 (propane and subsequent larger *n*-alkanes), P_2 (*iso*-butane), and P_3 (*neo*-pentane) where the subscript denotes the number of C atoms bonded to the NNN C atom of the C—H bond of interest. Similarly, one can envision 10 different types of secondaries, denoted as $S_{i,j}$, where *i* and *j* denote the numbers of C atoms bonded to the NNN C atoms from the secondary C—H bond of interest. For example, propane has two S_{00} secondary C—H bonds, and *n*-butane has four S_{01} secondary C—H bonds. One can then define 20 unique tertiary C—H bonds, $T_{i,j,k}$, using the above rule. However, even in the case of a primary C—H bond, there are inherent differences in the P_1 bonds in propane, as Hu et al.[55] postulated in their theoretical study on OH + C_3H_8. There are two different primary abstraction sites, an in-plane (trans) site and an out-of-plane (gauche) site with barrier heights that differ at the highest level of theory by ~0.5 kcal/mol. A recent study from this laboratory[20] (utilizing ab initio calculations for energetics at the G3//B3LYP[56] level) showed that the barrier heights for these two P_1 abstraction sites differ by 0.28 kcal/mol in C_3H_8 and by as much as 0.47 kcal/mol in the two distinct P_2 in- and out-of-plane sites in *i*-C_4H_{10}. Cohen's conventions[19] then have to be expanded such

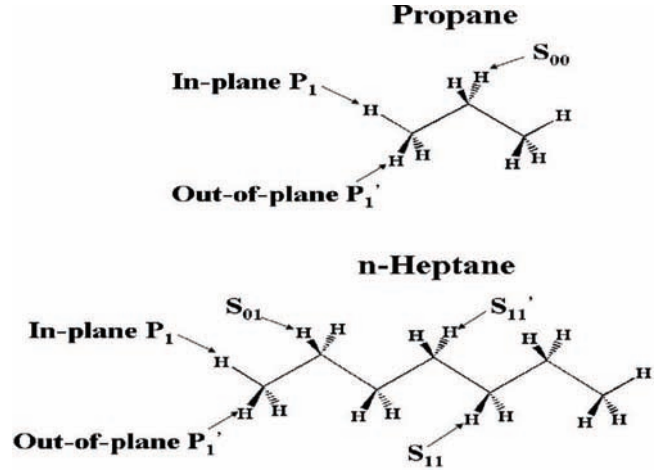

Figure 10. Types of primary and secondary C—H bonds in propane and *n*-heptane.

that there are two in-plane P_1 C—H bonds and four out-of-plane $P_{1'}$ C—H bonds in C_3H_8 and any larger *n*-alkane (see Figure 10). For any general alkane larger than ethane, there are then six possible primary abstraction sites; unique abstraction sites in P_0 and P_3 C—H bonds and two distinct in-plane and out-of plane sites in P_1 and P_2 C—H bonds. However, it will be difficult if not impossible to distinguish the in- and out-of-plane primary abstraction sites in an experiment. Furthermore, considering elementary reaction products, the in-plane and out-of-plane abstraction sites lead to the same 1-alkyl radical. Consequently, for the purposes of extracting group reactivities, we have assumed equivalency of the in-plane and out-of-plane contributions in the primary abstractions, P_1 and P_2.

As with the primary C—H bonds, there are unique in-plane and out-of-plane abstraction sites in secondary C—H bonds. For example, in recent work,[21] we observed that, for OH + methylcyclopentane, the in-plane and out-of-plane S_{12} abstraction sites (referred to as ortho S_1 and ortho S_2 sites in Figure 10[21]) differ in their barrier heights by 0.524 kcal/mol at the G3//B3LYP[56] level of theory. The corresponding in-plane and out-of-plane S_{11} abstraction sites (referred to as meta S_3 and meta S_4 sites in Figure 10[21]) differ by 0.218 kcal/mol, also at the G3//B3LYP[56] level of theory.

To confirm that there are additional secondary abstraction sites in *n*-alkanes other than Cohen's NNN configurations, ab initio electronic structure calculations were performed for OH + *n*-pentane and OH + *n*-heptane using the Gaussian 98[57] suite of programs. Geometric structures and vibration frequencies for the minima and saddle points were obtained utilizing density functional theory at the B3-LYP/6-31G(d) level. Transition states were verified by visualization of the imaginary frequency using MOLEKEL,[58] as well as by performing intrinsic reaction coordinate (IRC)[59] calculations. Subsequent higher-level energies were obtained at the G3//B3LYP[60] and QCISD(T,Full)/6-311G(d,p) levels of theory with the B3-LYP/6-31G(d) geometries. Appropriate scaling factors were used to scale the theoretically determined frequencies and zero-point-corrected energies.[60,61] Table 6 lists the barrier heights for the various abstraction sites for the reactions of OH with *n*-pentane and *n*-heptane. *n*-Heptane is the simplest alkane that includes all possible unique abstraction sites that are present in any *n*-alkane larger than *n*-butane. However, given the molecular size, barrier heights for OH + *n*-heptane could be obtained only at the QCISD(T,Full)/6-311G(d,p)//B3-LYP/6-31G(d) level of theory. Calculations performed at the same level of theory for the

TABLE 6: Barrier Heights[a] (kcal/mol) for Various H-Atom Abstraction Sites According to Next-Nearest-Neighbor Configurations[b]

reaction and level of theory	P_1[c]	$P_{1'}$[d]	S_{01}	S_{11}	$S_{11'}$[e]
n-pentane + OH QCISD(T,Full)/6-311G(d,p)//B3LYP/6-31G(d)	4.77	3.72	2.48	1.68	
n-heptane + OH QCISD(T,Full)/6-311G(d,p)//B3LYP/6-31G(d)	4.55	3.49	2.73	1.53	1.91
n-pentane + OH G3//B3LYP	1.98	1.79	0.84	0.40	

[a] Corrected for zero-point energy. [b] Classified in accordance with the work of Cohen,[19] who used a TST-based group-additivity model for H abstractions by OH from alkanes. [c] In-plane primary H atom. [d] Out-of-plane primary H atoms. [e] Secondary H atoms that do not neighbor S_{01} H atoms.

reaction of OH with *n*-pentane allowed comparison of barrier heights for similar abstraction sites. It is evident from Table 6 that there is a 0.4 kcal/mol difference in barrier heights at the QCISD(T,Full)/6-311G(d,p)//B3-LYP/6-31G(d) level of theory when abstracting from an S_{11} C—H bond neighboring an S_{01} C—H bond in comparison to an $S_{11'}$ C—H bond (that does not neighbor an S_{01} C—H bond) in *n*-heptane. Furthermore, abstraction from the same type of C—H bond occurs with similar barrier heights in *n*-pentane and *n*-heptane. With OH + *n*-pentane being a smaller molecular system, higher-level G3//B3LYP energetics were calculated in order to obtain more reliable estimates for the barrier heights for the various abstraction sites (see Table 6). One would expect similar barrier heights for the OH + *n*-heptane reaction if a higher level of theory (e.g., G3//B3LYP) were to be used. The ab initio calculations support the concept that accurate experimental data on a series of *n*-alkanes can be used to distinguish contributions from secondary S_{11} and $S_{11'}$ C—H abstractions.

***n*-Alkanes.** Considering secondary C—H bonds, Cohen's[19] method can be used up to *n*-hexane. *n*-Hexane has six P_1 (two in-plane P_1 and four out-of-plane $P_{1'}$ are averaged together as P_1) C—H bonds, four secondary S_{01} C—H bonds, and four secondary S_{11} C—H bonds. With Cohen's[19] method for *n*-heptane (Figure 10), there are then six P_1, four S_{01}, and six S_{11} C—H bonds, where it is assumed that the six S_{11} C—H bonds are equivalent. However, the ab initio calculations for *n*-heptane in Table 6 clearly demonstrate that the barrier heights for H abstraction from the S_{11} C—H bonds neighboring the S_{01} C—H bonds are different from that of the S_{11} C—H bond at the middle carbon atom, farther from the S_{01} C—H bonds. Furthermore, abstracting a H atom from the middle carbon atom in *n*-heptane leads to a different set of products, 4-heptyl + H_2O, in contrast to abstraction from its neighboring two carbon atoms, which leads to 3-heptyl + H_2O. Consequently, it is essential to distinguish the two distinct S_{11} abstraction sites, and we have designated the S_{11} C—H bond at the C_4 carbon atom as $S_{11'}$. Therefore, in *n*-heptane, there are three distinct secondary abstraction sites: four S_{01}, four S_{11}, and two $S_{11'}$ C—H bonds. Table 7 provides the updated classification of C—H bonds according to NNN configurations for a series of *n*-alkanes from ethane (C_2H_6) to *n*-cetane ($C_{16}H_{34}$). From Table 7, it is evident that reliable rate measurements for propane through *n*-heptane would be sufficient to obtain group estimates for individual P_1 (P_1 and $P_{1'}$ are assumed equivalent because they lead to the same products), S_{00}, S_{01}, S_{11}, and $S_{11'}$ abstractions that can then be used to make predictions for abstraction rates for large fuel-surrogate molecules such as *n*-cetane.

TABLE 7: Classification of *n*-Alkane C—H bonds According to Next-Nearest-Neighbor Configurations[a]

alkane	P_0	P_1[b]	$P_{1'}$[c]	S_{00}	S_{01}	S_{11}	$S_{11'}$[d]
ethane	6						
propane		2	4	2			
n-butane		2	4		4		
n-pentane		2	4		4	2	
n-hexane		2	4		4	4	
n-heptane		2	4		4	4	2
n-octane		2	4		4	4	4
n-nonane		2	4		4	4	6
n-decane		2	4		4	4	8
n-undecane		2	4		4	4	10
n-dodecane		2	4		4	4	12
n-tridecane		2	4		4	4	14
n-tetradecane		2	4		4	4	16
n-pentadecane		2	4		4	4	18
n-cetane		2	4		4	4	20

[a] Classification in accordance with the work of Cohen,[19] who used a TST-based group-additivity model for H abstractions by OH from alkanes. [b] In-plane primary H atom. [c] Out-of-plane primary H atoms. [d] Secondary H atoms that do not neighbor S_{01} H atoms.

In prior work in this laboratory,[20] the reactions of OH with four small alkanes, namely, propane, *n*-butane, *iso*-butane, and 2,2-dimethylpropane, were studied with the goals of (1) extending the measurements of Tully and co-workers[9−13] to higher temperatures and (2) obtaining more precise data (uncertainties within ±15%) than Bott and Cohen[14−16] over an extended temperature range encompassing combustion conditions. The high-*T* data were then utilized along with the other reported direct measurements to generate three-parameter fits of the rate constants over the temperature range from ~250 to 1300 K. The reported three-parameter fits are excellent representations of the available data and can be used to extract required *n*-alkane group values for P_1, S_{00}, and S_{01}. Droege and Tully[11] measured the branching ratios for primary and secondary abstractions in propane over the temperature range of 295−854 K. Their branching ratio, $\Phi = k_{primary}/k_{total}$, was fitted to a polynomial function to extend its range of validity to higher temperature, ~1300 K, over which the three-parameter evaluation for OH + propane is valid (eq 5 in the recent study[20]). Using this function, primary (P_1) and secondary (S_{00}) abstraction rate constants per H atom were extracted for OH + propane. These were then fitted to three-parameter expressions as

$$k/(\text{H atom } P_1) = 7.560\times10^{-18}T^{1.813}\exp(-437\text{ K}/T)\text{ cm}^3\text{ molecule}^{-1}\text{ s}^{-1} \quad (298-1300\text{ K}) \quad (11)$$

$$k/(\text{H atom } S_{00}) = 1.640\times10^{-17}T^{1.751}\exp(32\text{ K}/T)\text{ cm}^3\text{ molecule}^{-1}\text{ s}^{-1} \quad (298-1300\text{ K}) \quad (12)$$

With the *k*/(H atom) value derived for the P_1 abstraction (eq 11), the *k*/(H atom) value for the S_{01} abstraction in *n*-butane was obtained by utilizing the three-parameter fit to the rate constant for OH + *n*-butane (eq 6 in the recent study[20]). The *k*/(H atom) value for the S_{01} abstraction in *n*-butane was fitted to a three-parameter expression, giving

$$k/(\text{H atom } S_{01}) = 5.856\times10^{-15}T^{0.935}\exp(-254\text{ K}/T)\text{ cm}^3\text{ molecule}^{-1}\text{ s}^{-1} \quad (298-1300\text{ K}) \quad (13)$$

The present study reports rate constant measurements on larger *n*-alkanes (*n*-pentane through *n*-heptane), and we subse-

quently determined a three-parameter experimental evaluation for *n*-pentane (eq 8), which, along with the *k*/(H atom) values determined for P_1 (eq 11) and S_{01} (eq 13), was used to obtain the *k*/(H atom) value for abstraction from the S_{11} C—H bond as

$$k/(\text{H atom } S_{11}) = [\text{eq } 8 - 6(\text{eq } 11) - 4(\text{eq } 13)]/2 \quad (14)$$

This was then fitted to a three-parameter expression, giving

$$k/(\text{H atom } S_{11}) = 4.750\times10^{-18}T^{1.811}\exp(511\text{ K}/T)\text{ cm}^3\text{ molecule}^{-1}\text{ s}^{-1} \quad (298-1300\text{ K}) \quad (15)$$

With the derived group values for P_1, S_{01}, and S_{11} abstractions, a total rate constant prediction for the next largest *n*-alkane (*n*-hexane) was made. For *n*-hexane, the group method was applied as 6(eq 11) + 4(eq 13) + 4(eq 15), giving

$$k_{\text{OH+}n\text{-hexane,groups}} = 1.398\times10^{-16}T^{1.739}\exp(202\text{ K}/T)\text{ cm}^3\text{ molecule}^{-1}\text{ s}^{-1} \quad (298-1300\text{ K}) \quad (16)$$

The rate constants obtained using the group values (eq 16, plotted in Figure 8) are within ±10% of the experimental evaluation for OH + *n*-hexane (eq 9) over the temperature range of 298−1300 K. By contrast, as seen in Figure 8, Cohen's[19] recommendations for the OH + *n*-hexane total rate are 20−25% lower in the 500−1300 K range.

The only other unknown group required to make predictions for any *n*-alkane larger than *n*-hexane is the $S_{11'}$ group. In the present work, an experimental evaluation of the rate constants for OH + *n*-heptane over a wide temperature range (eq 6) was determined. The *k*/(H atom) value for abstraction from an $S_{11'}$ C—H bond was then calculated as

$$k/(\text{H atom } S_{11}') = [\text{eq } 6 - 6(\text{eq } 11) - 4(\text{eq } 13) - 4(\text{eq } 15)]/2 \quad (17)$$

The rate constants were then fitted to a three-parameter expression, giving

$$k/(\text{H atom } S_{11}') = 4.665\times10^{-13}T^{0.320}\exp(-426\text{ K}/T)\text{ cm}^3\text{ molecule}^{-1}\text{ s}^{-1} \quad (298-1300\text{ K}) \quad (18)$$

The *k*/(H atom) value for $S_{11'}$ deviates from that for S_{11} by as much as ±49%, with the largest deviations at the intermediate temperatures, 600−700 K. This completes the three-parameter fits to the groups required for predicting OH + *n*-alkane for any *n*-alkane.

To illustrate, total rate constants for OH + *n*-heptane can be obtained as 6(eq 11) + 4(eq 13) + 4(eq 15) + 2(eq 18), giving

$$k_{\text{OH+}n\text{-heptane,groups}} = 9.906\times10^{-16}T^{1.497}\exp(96\text{ K}/T)\text{ cm}^3\text{ molecule}^{-1}\text{ s}^{-1} \quad (298-1300\text{ K}) \quad (19)$$

This estimate for the total rate constants for OH + *n*-heptane is in excellent agreement with the experimental evaluation (eq 6), being within ±10% over the temperature range of 300−1300 K. However, the present estimate (eq 19) predicts rate constants that are larger than Cohen's[19] recommendation by as much as 35% at 700 K, with deviations greater than ±23% over the 500−1300 K range (see Figure 3).

To make predictions for larger *n*-alkanes, the available literature data on reactions of OH with *n*-octane, *n*-nonane, and *n*-decane were used to obtain experimental evaluations. For OH + *n*-octane, the evaluation included the measurements of Koffend and Cohen[17] (1078 K), Wilson et al.[33] (284−393 K), Greiner[37] (296−497 K), Li et al.[62] (240−340 K), Atkinson et al.[35] (299 K), Anderson et al.[32] (295 K), Anderson et al.[34] (296 K), and Nolting et al.[44] (312 K). The resultant 20 points from the eight OH + *n*-octane studies (five studies were single-temperature values) were then fitted to a three-parameter expression, giving

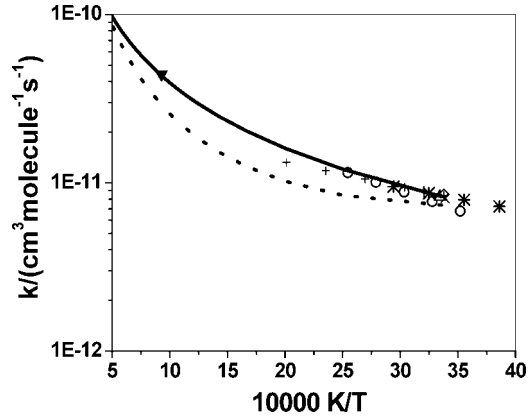

Figure 11. Arrhenius plot of the OH + *n*-octane rate constants. (—) Three-parameter fit to groups, present work, 298−2000 K, eq 21; (• • •) Cohen,[19] TST total rate, 298−2000 K; (▼) Koffend and Cohen,[17] 1078 K; (○) Wilson et al.,[33] 220−407 K; (Δ) Atkinson et al.,[35] 299 K; (×) Anderson et al.,[32] 295 K; (◊) Anderson et al.,[34] 296 K; (+) Greiner,[37] 296−497 K; (l) Nolting et al.,[44] 312 K; (*) Li et al.,[62] 240−340 K.

$$k_{\text{OH+}n\text{-octane}} = 1.124\times10^{-16}T^{1.809}\exp(264\text{ K}/T)\text{ cm}^3\text{ molecule}^{-1}\text{ s}^{-1} \quad (240-1180\text{ K}) \quad (20)$$

The rate constants for OH + *n*-octane using group estimates can be obtained as 6(eq 11) + 4(eq 13) + 4(eq 15) + 4(eq 18), giving

$$k_{\text{OH+}n\text{-octane,groups}} = 4.186\times10^{-15}T^{1.322}\exp(19\text{ K}/T)\text{ cm}^3\text{ molecule}^{-1}\text{ s}^{-1} \quad (298-1200\text{ K}) \quad (21)$$

In Figure 11, the Arrhenius plot for OH + *n*-octane is shown. The group estimates given by eq 21 are within ±10% of the experimental evaluation (eq 20). However, Cohen's[19] recommendation for this rate constant shows large deviations, being 63% lower than the present estimate at 700 K and exhibiting deviations of >30% over the 400−1500 K range (see Figure 11). The present group estimates are in excellent agreement with the only high-*T* data of Koffend and Cohen[17] at 1078 K, with Cohen's earlier TST recommendation[19] being ∼50% lower.

For OH + *n*-nonane, the experimental evaluation includes the data of Koffend and Cohen[17] (1097 K), Atkinson et al.[35] (299 K), Nolting et al.[44] (312 K), Li et al.[62] (240−340 K), Ferrari et al.[31] (296 K), Kramp and Paulson[63] (296 K), Behnke et al.[64] (300 K), Colomb et al.[65] (294 K), and Coeur et al.[66] (295 K). The resultant 13 points from the nine OH + *n*-nonane studies (eight studies were single-*T* values) were then fitted to a three-parameter expression, giving

$$k_{\text{OH+}n\text{-nonane}} = 1.370\times10^{-14}T^{1.158}\exp(-2\text{ K}/T)\text{ cm}^3\text{ molecule}^{-1}\text{ s}^{-1} \quad (240-1097\text{ K}) \quad (22)$$

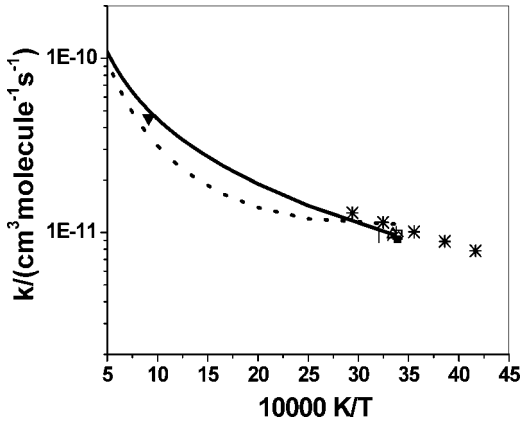

Figure 12. Arrhenius plot of the OH + *n*-nonane rate constants. (—) Three-parameter fit to groups, present work, 298−2000 K, eq 23; (• • •) Cohen,[19] TST total rate, 298−2000 K; (▼) Koffend and Cohen,[17] 1097 K; (□) Ferrari et al.,[31] 295 K; (Δ) Atkinson et al.,[35] 299 K; (×) Behnke et al.,[64] 300 K; (◊) Colomb et al.,[65] 294 K; (+) Kramp and Paulson,[63] 296 K; (l) Nolting et al.,[44] 312 K; (■) Coeur et al.,[66] 295 K; (*) Li et al.,[62] 240−340 K.

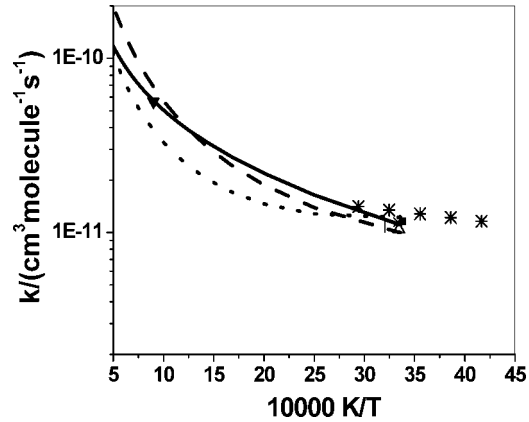

Figure 13. Arrhenius plot of the OH + *n*-decane rate constants. (—) Three-parameter fit to groups, present work, 298−2000 K, eq 25; (• • •) Cohen,[19] TST total rate, 298−2000 K, (− − −) Kwok and Atkinson[68] scheme, 298−2000 K; (▼) Koffend and Cohen,[17] 1109 K; (Δ) Atkinson et al.,[35] 299 K; (×) Behnke et al.,[64] 300 K; (l) Nolting et al.,[44] 312 K; (■) Aschmann et al.,[67] 296 K; (*) Li et al.,[62] 240−340 K.

The rate constants for OH + *n*-nonane using group estimates can be obtained as 6(eq 11) + 4(eq 13) + 4(eq 15) + 6(eq 18), giving

$$k_{\mathrm{OH}+n\text{-nonane,groups}} = 1.290\times10^{-14}T^{1.186}\exp(-40\ \mathrm{K}/T)\ \mathrm{cm^3\ molecule^{-1}\ s^{-1}} \quad (298-1100\ \mathrm{K})\ (23)$$

Figure 12 is an Arrhenius plot for OH + *n*-nonane. The group estimates (eq 23) lie within ±10% of the experimental evaluation for OH + *n*-nonane (eq 22). Again, large deviations, of more than ±35%, are observed over the temperature range of 500−1100 K between the present group estimates and Cohen's recommendations[19] for OH + *n*-nonane (see Figure 12). In contrast to the excellent prediction made by the present group method, Cohen's TST[19] recommendation is 36% lower than the only available high-*T* data of Koffend and Cohen[17] at 1097 K.

For OH + *n*-decane the experimental evaluation included the data of Koffend and Cohen[17] (1109 K), Li et al.[62] (240−340 K), Atkinson et al.[35] (299 K), Nolting et al.[44] (312 K), Behnke et al.[64] (300 K), and Aschmann et al.[67] (296 K). The resultant 10 points from the six OH + *n*-decane studies (five studies were single-*T* values) were then fitted to a three-parameter expression, giving

$$k_{\mathrm{OH}+n\text{-decane}} = 6.747\times10^{-18}T^{2.203}\exp(550\ \mathrm{K}/T)\ \mathrm{cm^3\ molecule^{-1}\ s^{-1}} \quad (240-1109\ \mathrm{K})\ (24)$$

The rate constants for OH + *n*-decane using group estimates can be obtained as 6(eq 11) + 4(eq 13) + 4(eq 15) + 8(eq 18), giving

$$k_{\mathrm{OH}+n\text{-decane,groups}} = 3.012\times10^{-14}T^{1.087}\exp(-84\ \mathrm{K}/T)\ \mathrm{cm^3\ molecule^{-1}\ s^{-1}} \quad (298-1100\ \mathrm{K})\ (25)$$

The Arrhenius plot for OH + *n*-decane is shown in Figure 13. For OH + *n*-decane, the group scheme (eq 25) predicts rate constants that are 12% higher than the experimental evaluation (eq 24) at ~500 K, with smaller deviations at higher and lower temperatures. Cohen's TST recommendation[19] is 46% lower than the single-*T* value of Koffend and Cohen[17] at 1109 K, as seen in Figure 13. On the other hand, the present group scheme (eq 25) predicts a rate constant that is only 1% higher than that of Koffend and Cohen.[17] For OH + *n*-decane, we also made comparisons against a simpler model developed by Kwok and Atkinson,[68] which assumes the equivalency of all primary, secondary, and tertiary H atoms. As seen in Figure 13, the Kwok and Atkinson model[68] predicts a rate constant that is 20% higher than the single-*T* value of Koffend and Cohen[17] at 1109 K. Their simpler model predicts a rate constant that is lower than the present group scheme (eq 25) by 10% at 298 K and is 25−70% higher in the temperature range of 1200−2000 K. For nearly all of the other cases considered here, the Kwok and Atkinson[68] model is less accurate than the present group scheme, especially at combustion temperatures. Within experimental error, our group scheme predicts accurate values over a wide temperature range for OH reactions with *n*-alkanes up to *n*-decane. For larger *n*-alkanes (C_{11}−C_{16}) the only available data[69] are the measurements of Nolting et al.[44] (312 K) and Behnke et al.[64] (300 K). Using the groups, the predicted rate constants for these larger alkanes are

$$k_{\mathrm{OH}+n\text{-undecane}} = 5.284\times10^{-14}T^{1.025}\exp(-111\ \mathrm{K}/T)\ \mathrm{cm^3\ molecule^{-1}\ s^{-1}} \quad (298-1300\ \mathrm{K})\ (25b)$$

$$k_{\mathrm{OH}+n\text{-dodecane}} = 9.325\times10^{-14}T^{0.960}\exp(-139\ \mathrm{K}/T)\ \mathrm{cm^3\ molecule^{-1}\ s^{-1}} \quad (298-1300\ \mathrm{K})\ (26)$$

$$k_{\mathrm{OH}+n\text{-tridecane}} = 1.508\times10^{-13}T^{0.907}\exp(-163\ \mathrm{K}/T)\ \mathrm{cm^3\ molecule^{-1}\ s^{-1}} \quad (298-1300\ \mathrm{K})\ (27)$$

$$k_{\mathrm{OH}+n\text{-tetradecane}} = 2.278\times10^{-13}T^{0.862}\exp(-183\ \mathrm{K}/T)\ \mathrm{cm^3\ molecule^{-1}\ s^{-1}} \quad (298-1300\ \mathrm{K})\ (28)$$

$$k_{\mathrm{OH}+n\text{-pentadecane}} = 3.262\times10^{-13}T^{0.823}\exp(-201\ \mathrm{K}/T)\ \mathrm{cm^3\ molecule^{-1}\ s^{-1}} \quad (298-1300\ \mathrm{K})\ (29)$$

$$k_{OH+n\text{-cetane}} = 4.474\times10^{-13}T^{0.789}\exp(-216\ \mathrm{K}/T)\ \mathrm{cm^3\ molecule^{-1}\ s^{-1}}\quad(298-1300\ \mathrm{K})\quad(30)$$

The rate constants at 298 K for *n*-undecane through *n*-tridecane, using eqs 25 − 27, are within ±5% of the recommendations of Atkinson.[69] For *n*-tetradecane through *n*-cetane, the rate constants at 312 K, using eqs 28−30, lie within ±12% of Atkinson's recommendations.[69]

The groups extracted using experimental evaluations from 298 to 1300 K appear to be reliable enough to predict values for larger *n*-alkanes (>C_{16}) not considered here. A summary of the rate parameters for the groups determined from this work is listed in Table 8. These group values from experimental data over the temperature range from 298 to 1300 K appear to be reliable for extrapolation to higher flame temperatures. The applicability was therefore tested for higher temperatures by comparing against Cohen's[19] TST estimates for 298−2000 K. Despite larger deviations in the intermediate temperature range of 500−1500 K, Cohen's[19] TST-based predictions at 2000 K are within ±15% of those calculated from the three-parameter experimental evaluations for propane (eq 5[20]), *n*-pentane (eq 8), *n*-hexane (eq 9), *n*-heptane (eq 6), *n*-octane (eq 20), *n*-nonane (eq 22), and *n*-decane (eq 24). A larger deviation with temperature is observed only for *n*-butane using Cohen's[19] 2000 K prediction (27% higher than the evaluation in eq 6[20]). The groups derived from data over a wide temperature range (298−1300 K) in this work can be extrapolated to 2000 K without much error.

Table 8 can then be used to obtain the rate parameters for individual abstraction channels leading to a given alkyl radical + H_2O for any *n*-alkane. For example, in the case of *n*-heptane, the rate expressions for the groups P_1, S_{01}, S_{11}, and $S_{11'}$ (in Table 8) multiplied by the corresponding path degeneracy factors of 6, 4, 4, and 2 give the rate expressions that lead to 1-heptyl + H_2O, 2-heptyl + H_2O, 3-heptyl + H_2O, and 4-heptyl + H_2O, respectively, as

$$k_{1\text{-heptyl}+H_2O} = 4.536\times10^{-17}T^{1.813}\exp(-437\ \mathrm{K}/T)\ \mathrm{cm^3\ molecule^{-1}\ s^{-1}}\quad(298-2000\ \mathrm{K})\quad(31)$$

$$k_{2\text{-heptyl}+H_2O} = 2.342\times10^{-14}T^{0.935}\exp(-254\ \mathrm{K}/T)\ \mathrm{cm^3\ molecule^{-1}\ s^{-1}}\quad(298-2000\ \mathrm{K})\quad(32)$$

$$k_{3\text{-heptyl}+H_2O} = 1.900\times10^{-17}T^{1.811}\exp(511\ \mathrm{K}/T)\ \mathrm{cm^3\ molecule^{-1}\ s^{-1}}\quad(298-2000\ \mathrm{K})\quad(33)$$

TABLE 8: Summary of Rate Parameters for Each Group According to the Expression $k = AT^n \exp(-B/T)$ cm^3 molecule^{-1} s^{-1}

group	*A*	*n*	*B*
P_0	4.467×10^{-19}	2.224	373
P_1	7.560×10^{-18}	1.813	437
P_2	9.267×10^{-19}	2.078	189
P_3	9.087×10^{-18}	1.763	374
S_{00}	1.640×10^{-17}	1.751	−32
S_{01}	5.856×10^{-15}	0.935	254
S_{11}	4.750×10^{-18}	1.811	−511
$S_{11'}$	4.665×10^{-13}	0.320	426
T_{000}	8.044×10^{-18}	1.840	−503
T_{002}	7.841×10^{-14}	0.576	−35

$$k_{4\text{-heptyl}+H_2O} = 9.330\times10^{-13}T^{0.320}\exp(-426\ \mathrm{K}/T)\ \mathrm{cm^3\ molecule^{-1}\ s^{-1}}\quad(298-2000\ \mathrm{K})\quad(34)$$

The branching ratios in OH + *n*-heptane leading to the various radicals are plotted in Figure 14. At the highest temperature, 2000 K, branching ratios in OH + *n*-heptane are nearly equivalent to the ratios of the path degeneracy for a given channel to that for all paths.

***iso*-Alkanes.** In the earlier section on *n*-alkanes, experimental data were used to distinguish the contributions from various types of secondary C—H bonds. Using similar methods, experimental data were used to differentiate contributions from tertiary C—H bonds. In prior work from this laboratory,[20] the reaction of OH with *iso*-butane was studied. *iso*-Butane has nine P_2 primary C—H bonds and a single tertiary T_{000} C—H bond. Theoretical predictions of the branching ratios for primary abstractions were shown to be in excellent agreement with the measurements of Tully et al.[12]

As in the earlier section on *n*-alkanes, the experimental branching ratios of Tully et al.,[12] extrapolated to a higher temperature range (1300 K) by means of a polynomial function, were employed and subsequently used to obtain the rates of P_2 primary abstraction and T_{000} tertiary abstraction in *iso*-butane. These were then fitted to three-parameter expressions as

$$k/(\mathrm{H\ atom\ P_2}) = 9.267\times10^{-19}T^{2.078}\exp(-189\ \mathrm{K}/T)\ \mathrm{cm^3\ molecule^{-1}\ s^{-1}}\quad(298-1300\ \mathrm{K})\quad(35)$$

$$k/(\mathrm{H\ atom\ T_{000}}) = 8.044\times10^{-18}T^{1.840}\exp(503\ \mathrm{K}/T)\ \mathrm{cm^3\ molecule^{-1}\ s^{-1}}\quad(298-1300\ \mathrm{K})\quad(36)$$

In this study, rate constant measurements on OH + 2,3-DMB are reported, and this is the next higher homologue in the series of alkanes that has only primary and tertiary C—H bonds. A three-parameter experimental evaluation for this reaction (eq 10) was determined, which, along with the *k*/(H atom) value determined for P_2 (eq 35), was used to obtain the *k*/(H atom) for abstraction from the T_{002} C—H bond as

$$k/(\mathrm{H\ atom\ T_{002}}) = [\mathrm{eq\ 10} - 12(\mathrm{eq\ 35})]/2 \qquad (37)$$

The result was then fitted to a three-parameter expression, giving

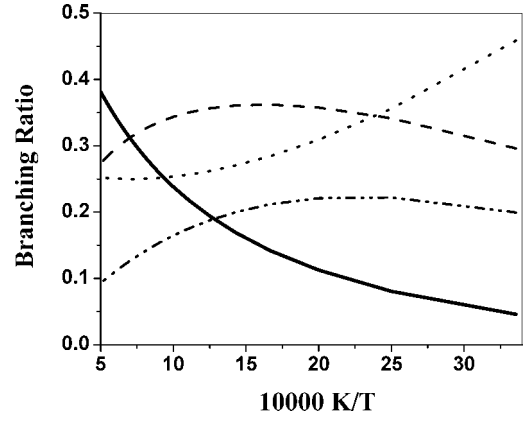

Figure 14. Branching ratios (298−2000 K) leading to the various heptyl products in OH + *n*-heptane. (—) $k_{1\text{-heptyl}+H_2O}$ (eq 31)/$k_{OH+n\text{-heptane}}$ (eq 19), (− − −) $k_{2\text{-heptyl}+H_2O}$ (eq 32)/$k_{OH+n\text{-heptane}}$ (eq 19), (• • •) $k_{3\text{-heptyl}+H_2O}$ (eq 33)/$k_{OH+n\text{-heptane}}$ (eq 19), (— •• —) $k_{4\text{-heptyl}+H_2O}$ (eq 34)/$k_{OH+n\text{-heptane}}$ (eq 19).

$$k/(\text{H atom } T_{002}) = 7.841\times10^{-14}T^{0.576}\exp(35\text{ K}/T)\text{ cm}^3\text{ molecule}^{-1}\text{ s}^{-1} \quad (298-1300\text{ K}) \quad (38)$$

A comparison of eqs 36 and 38 shows significant differences between the abstraction rate constants from the two tertiary C—H bonds (T_{000} and T_{002}). At room temperature (298 K, where the contributions from these tertiary abstractions are expected to dominate), abstraction from the T_{000} bond (eq 36) is ~50% lower than that from the T_{002} bond. The deviations at higher temperatures are lower. Cohen's[19] TST prediction is ~60% lower than the value obtained by Bott and Cohen[16] at 1220 K (see Figure 9).

***neo*-Alkanes.** *neo*-Alkanes represent the simplest class of alkanes because they have only one unique primary C—H bond, namely, a P_3 bond. Hence, the two simplest *neo*-alkanes, *neo*-pentane and *neo*-octane, have been the focus of several kinetics studies.[69] In recent work from this laboratory,[20] OH + 2,2-dimethylpropane was studied experimentally, and theoretical calculations were in excellent agreement with the data over a wide temperature range. The present work reports measurements on OH + 2,2,3,3-TMB. We utilized the average of the three-parameter experimental evaluations for 2,2-dimethylpropane (eq 8)[20] and 2,2,3,3-TMB (eq 7) to obtain the group value for abstraction from a P_3 C—H bond as

$$k/(\text{H atom } P_3) = [(\text{eq } 8)/12 + (\text{eq } 7)/18]/2 \quad (39)$$

The result was then fitted to a three-parameter expression, giving

$$k/(\text{H atom } P_3) = 9.087\times10^{-18}T^{1.763}\exp(-374\text{ K}/T)\text{ cm}^3\text{ molecule}^{-1}\text{ s}^{-1} \quad (298-1300\text{ K}) \quad (40)$$

Cohen's TST prediction[19] for OH + 2,2-dimethylpropane at room temperature is 26% higher than the present group estimate [12(eq 40)] and is 21—26% lower in the high-T range (900—1300 K). The rate constants for OH + 2,2,3,3-TMB using group estimates can be obtained as 18(eq 40), giving

$$k_{\text{OH+2,2,3,3-TMB, groups}} = 1.636\times10^{-16}T^{1.763}\exp(-374\text{ K}/T)\text{ cm}^3\text{ molecule}^{-1}\text{ s}^{-1} \quad (298-1300\text{ K}) \quad (41)$$

For OH + 2,2,3,3-TMB, Cohen's TST predictions[19] are 21—28% lower than the present group values (eq 41) in the 700—1300 K range, with decreasing deviations at even lower temperatures (see Figure 6). The group value for a P_0 primary C—H bond can be obtained from the three-parameter experimental evaluation for OH + C_2H_6 in prior work from this laboratory[70] and is shown in Table 8 for completeness along with the other group values.

The experimental database at present is able to distinguish that the rates of abstraction are different at various primary, secondary, and tertiary sites. The available data have been used to obtain groups from NNN configurations for H-atom abstractions by OH for four primary, four secondary, and two tertiary C—H bonds. These group values are summarized in Table 8, and their validity extends from 298—2000 K. For convenience, in Table 9, we summarize the predicted Arrhenius parameters for total rate constants for all molecules considered in this work. We recommend that these total rate constants and group values be used in combustion modeling.

TABLE 9: Summary of Rate Parameters for Total Rate Constants (298—2000 K) According to the Expression $k = AT^n\exp(-B/T)$ cm^3 molecule^{-1} s^{-1}

molecule	A	n	B
ethane	2.680×10^{-18}	2.224	373
propane	2.419×10^{-17}	1.935	91
n-butane	8.499×10^{-16}	1.475	139
i-butane	6.309×10^{-19}	2.414	−381
n-pentane	2.495×10^{-16}	1.649	−80
neo-pentane	1.090×10^{-16}	1.763	374
n-hexane	1.398×10^{-16}	1.739	−202
2,3-dimethylbutane	2.287×10^{-17}	1.958	−365
n-heptane	9.906×10^{-16}	1.497	−96
n-octane	4.186×10^{-15}	1.322	−19
neo-octane	1.636×10^{-16}	1.763	374
n-nonane	1.290×10^{-14}	1.186	40
n-decane	3.012×10^{-14}	1.087	84
n-undecane	5.284×10^{-14}	1.025	111
n-dodecane	9.325×10^{-14}	0.960	139
n-tridecane	1.508×10^{-13}	0.907	163
n-tetradecane	2.278×10^{-13}	0.862	183
n-pentadecane	3.262×10^{-13}	0.823	201
n-hexadecane	4.474×10^{-13}	0.789	216

Conclusions

High-T rate constants for H abstractions by OH from five large alkanes (*n*-pentane, *n*-hexane, 2,3-DMB, *n*-heptane, and 2,2,3,3-TMB) have been measured with the reflected-shock-tube technique using multipass absorption spectrometric detection of OH. These experiments are the first direct measurements at $T > 800$ K for *n*-pentane and the only T-dependent data at high T (>800 K) for the other alkanes studied in this work. The high-temperature data have been combined with prior lower-temperature and room-temperature measurements to generate three-parameter rate constant evaluations. A simple group scheme was devised on the basis of the three-parameter experimental evaluations. The group scheme is able to make excellent predictions for the rate constants for H abstractions by OH from a series of *n*-alkanes (C_3—C_{16}) over a wide temperature range and represents an improvement over Cohen's TST-based group scheme. We recommend that these group values be used in combustion modeling.

Acknowledgment. This work was supported by the U.S. Department of Energy, Office of Basic Energy Sciences, Division of Chemical Sciences, Geosciences, and Biosciences, under Contract DE-AC02-06CH11357. The authors thank Drs. L. B. Harding and S. J. Klippenstein for their insightful comments.

References and Notes

(1) Pitz, W. J.; Cernansky, N. P.; Dryer, F. L.; Egolfopoulos, F. N.; Farrell, J. T.; Friend, D. G.; Pitsch, H. *Development of an Experimental Database and Kinetic Models for Surrogate Gasoline Fuels*; SAE Paper 2007-01-0175; SAE International: Warrendale, PA, 2007.

(2) Farrell, J. T.; Cernansky, N. P.; Dryer, F. L.; Friend, D. G.; Hergart, C.-A.; Law, C. K.; McDavid, R. M.; Mueller, C. J.; Patel, A. K.; Pitsch, H. *Development of an Experimental Database and Kinetic Models for Surrogate Diesel Fuels*; SAE Paper 2007-01-0201; SAE International: Warrendale, PA, 2007.

(3) Colket, M.; Edwards, T.; Williams, S.; Cernansky, N. P.; Miller, D. L.; Egolfopoulos, F.; Lindstedt, P.; Seshadri, K.; Dryer, F. L.; Law, C. K.; Friend, D.; Lenhert, D. B.; Pitsch, H.; Sarofim, A.; Smooke, M.; Tsang, W. *Development of an Experimental Database and Kinetic Models for Surrogate Jet Fuels*; AIAA Paper AIAA-2007-0770; AIAA: Reston, VA, 2007.

(4) Dagaut, P.; Gail, S.; Sahasrabudhe, M. *Proc. Combust. Inst.* **2007**, *31*, 2955.

(5) Herbinet, O.; Pitz, W. J.; Westbrook, C. K. *Combust. Flame* **2008**, *154*, 507.
(6) Blake, D. R.; Rowland, F. S. *Science* **1995**, *269*, 953–956.
(7) Glassman, I. Combustion, 3rd ed.; Academic Press: San Diego, CA, 1996; p 94.
(8) Manion, J. A.; Huie, R. E.; Levin, R. D.; Burgess, D. R., Jr.; Orkin, V. L.; Tsang, W.; McGivern, W. S.; Hudgens, J. W.; Knyazev, V. D.; Atkinson, D. B.; Chai, E.; Tereza, A. M.; Lin, C.-Y.; Allison, T. C.; Mallard, W. G.; Westley, F.; Herron, J. T.; Hampson, R. F.; Frizzell, D. H. *NIST Chemical Kinetics Database*; NIST Standard Reference Database 17; version 7.0 (web version), release 1.4; National Institute of Standards and Technology (NIST): Gaithersburg, MD, 2000; available at http://kinetics.nist.gov.
(9) Tully, F. P.; Koszykowski, M. L.; Binkley, J. S. *Proc. Combust. Inst.* **1984**, *23*, 715–721.
(10) Tully, F. P.; Droege, A. T.; Koszykowski, M. L.; Melius, C. F. *J. Phys. Chem.* **1986**, *90*, 691–698.
(11) Droege, A. T.; Tully, F. P. *J. Phys. Chem.* **1986**, *90*, 1949–1954.
(12) Tully, F. P.; Goldsmith, J. E. M.; Droege, A. T. *J. Phys. Chem.* **1986**, *90*, 5932–5937.
(13) Droege, A. T.; Tully, F. P. *J. Phys. Chem.* **1986**, *90*, 5937–5941.
(14) Bott, J. F.; Cohen, N. *Int. J. Chem. Kinet.* **1984**, *16*, 1557–1566.
(15) Bott, J. F.; Cohen, N. *Int. J. Chem. Kinet.* **1989**, *21*, 485–498.
(16) Bott, J. F.; Cohen, N. *Int. J. Chem. Kinet.* **1991**, *23*, 1075–1094.
(17) Koffend, I. B.; Cohen, N. *Int. J. Chem. Kinet.* **1996**, *28*, 79–87.
(18) Cohen, N. *Int. J. Chem. Kinet.* **1982**, *14*, 1339–1362.
(19) Cohen, N. *Int. J. Chem. Kinet.* **1991**, *23*, 397–417.
(20) Sivaramakrishnan, R.; Srinivasan, N. K.; Su, M.-C.; Michael, J. V. *Proc. Combust. Inst.* **2009**, *32* (1), 107–114.
(21) Sivaramakrishnan, R.; Michael, J. V. *Combust. Flame*, **2009**, *156* (5), 1126−1134.
(22) Michael, J. V. *Prog. Energy Combust. Sci.* **1992**, *18*, 327–347.
(23) Michael, J. V. In *Advances in Chemical Kinetics and Dynamics*; Barker, J. R., Ed.; JAI Press: Stamford, CT, 1992; Vol. 1, pp 47−112, for original references.
(24) Michael, J. V.; Sutherland, J. W. *Int. J. Chem. Kinet.* **1986**, *18*, 409–436.
(25) Michael, J. V. *J. Chem. Phys.* **1989**, *90*, 189–198.
(26) Michael, J. V.; Fisher, J. R. In *Seventeenth International Symposium on Shock Waves and Shock Tube, AIP Conference Proceedings 208*; Kim, Y. W., Ed.; American Institute of Physics: New York, 1990; pp 210−215.
(27) Su, M.-C.; Kumaran, S. S.; Lim, K. P.; Michael, J. V. *Rev. Sci. Instrum.* **1995**, *66*, 4649–4654.
(28) Su, M.-C.; Kumaran, S. S.; Lim, K. P.; Michael, J. V.; Wagner, A. F.; Harding, L. B.; Fang, D.-C. *J. Phys. Chem. A* **2002**, *106*, 8261–8270.
(29) Srinivasan, N. K.; Su, M.-C.; Sutherland, J. W.; Michael, J. V. *J. Phys. Chem. A* **2005**, *109*, 1857–1863.
(30) Srinivasan, N. K.; Su, M.-C.; Michael, J. V. *J. Phys. Chem. A* **2007**, *111*, 3951–3958.
(31) Ferrari, C.; Roche, A.; Jacob, V.; Foster, P.; Baussand, P. *Int. J. Chem. Kinet.* **1996**, *28*, 609–614.
(32) Anderson, R. S.; Czuba, E.; Ernst, D.; Huang, L.; Thompson, A. E.; Rudolph, J. *J. Phys. Chem. A* **2003**, *107*, 6191–6199.
(33) Wilson, E. W.; Hamilton, W. A.; Kennington, H. R.; Evans, B.; Scott, M. W.; DeMore, W. B. *J. Phys. Chem. A* **2006**, *110*, 3593–3604.
(34) Anderson, R. S.; Huang, L.; Iannone, R.; Thompson, A. E.; Rudolph, J. *J. Phys. Chem. A* **2004**, *108*, 11537–11544.
(35) Atkinson, R.; Aschmann, S. M.; Carter, W. P. L.; Winer, A. M.; Pitts, J. N. *Int. J. Chem. Kinet.* **1982**, *14*, 781–788.
(36) Klopffer, W.; Frank, R.; Kohl, E.-G.; Haag, F. *Chem. Z.* **1986**, *110*, 57–62.
(37) Greiner, N. R. *J. Chem. Phys.* **1970**, *53*, 1070–1076.
(38) Atkinson, R.; Carter, W. P. L.; Aschmann, S. M.; Winer, A. M.; Pitts, J. N., Jr. *Int. J. Chem. Kinet.* **1984**, *16*, 469–481.
(39) DeMore, W. B.; Bayes, K. D. *J. Phys. Chem. A* **1999**, *103*, 2649–2654.
(40) Donahue, N. M.; Anderson, J. G.; Demerjian, K. L. *J. Phys. Chem. A* **1998**, *102*, 3121–3126.
(41) Talukdar, R. K.; Melouki, A.; Gierczak, T.; Barone, S.; Chiang, S.-Y.; Ravishankara, A. R. *Int. J. Chem. Kinet.* **1994**, *26*, 973–990.
(42) Iannone, R.; Anderson, R. S.; Vogel, A.; Rudolph, J.; Eby, P.; Whiticar, M. J. *J. Atmos. Chem.* **2004**, *47*, 191–208.
(43) Abbatt, J. P. D.; Demerjian, K. L.; Anderson, J. G. *J. Phys. Chem.* **1990**, *94*, 4566–4575.
(44) Nolting, F.; Behnke, W.; Zetzsch, C. *J. Atmos. Chem.* **1988**, *6*, 47–59.
(45) Cox, R. A.; Derwent, R. G.; Williams, M. R. *Environ. Sci. Technol.* **1980**, *14*, 57–61.
(46) Darnall, K. R.; Atkinson, R.; Pitts, J. N., Jr. *J. Phys. Chem.* **1978**, *82*, 1581–1584.
(47) McLoughlin, P.; Kane, R.; Shanahan, I. *Int. J. Chem. Kinet.* **1993**, *25*, 137–149.
(48) Barnes, I.; Bastian, V.; Becker, K. H.; Fink, E. H.; Nelsen, W. *J. Atmos. Chem.* **1986**, *4*, 445–466.
(49) Lloyd, A. C.; Darnall, K. R.; Winer, A. M.; Pitts, J. N., Jr. *J. Phys. Chem.* **1976**, *80*, 789–794.
(50) Campbell, I. M.; McLaughlin, D. F.; Handy, B. J. *Chem. Phys. Lett.* **1976**, *38*, 362–364.
(51) Darnall, K. R.; Winer, A. M.; Lloyd, A. C.; Pitts, J. N., Jr. *Chem. Phys. Lett.* **1976**, *44*, 415–418.
(52) Benson, S. W. *Thermochemical Kinetics*, John Wiley & Sons, Inc., 1968.
(53) Baldwin, R. R.; Walker, R. W. *J. Chem. Soc. Farad. Trans. I* **1979**, *75*, 140.
(54) Huynh, L. K.; Ratkiewicz, A.; Truong, T. N. *J. Phys. Chem. A* **2006**, *110*, 473.
(55) Hu, W.-P.; Rossi, I.; Corchado, J. C.; Truhlar, D. G. *J. Phys. Chem. A* **1997**, *101*, 6911.
(56) Baboul, A. G.; Curtiss, L. A.; Redfern, P. C.; Raghavachari, K. *J. Chem. Phys.* **1999**, *110*, 7650.
(57) Frisch, M. J.; Trucks, G. W.; Schlegel, H. B.; Scuseria, G. E.; Robb, M. A.; Cheeseman, J. R.; Zakrzewski, V. G.; Montgomery, J. A., Jr.; Stratmann, R. E.; Burant, J. C.; Dapprich, S.; Millam, J. M.; Daniels, A. D.; Kudin, K. N.; Strain, M. C.; Farkas, O.; Tomasi, J.; Barone, V.; Cossi, M.; Cammi, R.; Mennucci, B.; Pomelli, C.; Adamo, C.; Clifford, S.; Ochterski, J.; Petersson, G. A.; Ayala, P. Y.; Cui, Q.; Morokuma, K.; Malick, D. K.; Rabuck, A. D.; Raghavachari, K.; Foresman, J. B.; Cioslowski, J.; Ortiz, J. V.; Baboul, A. G.; Stefanov, B. B.; Liu, G.; Liashenko, A.; Piskorz, P.; Komaromi, I.; Gomperts, R.; Martin, R. L.; Fox, D. J.; Keith, T.; Al-Laham, M. A.; Peng, C. Y.; Nanayakkara, A.; Gonzalez, C.; Challacombe, M.; Gill, P. M. W.; Johnson, B.; Chen, W.; Wong, M. W.; Andres, J. L.; Head-Gordon, M.; Replogle, E. S.; Pople, J. A. *Gaussian 98*, revision A.7; Gaussian, Inc.: Pittsburgh, PA, 1998.
(58) Flükiger, P.; Lüthi, H. P.; Portmann, S.; Weber, J. *MOLEKEL 4.2*; Swiss Center for Scientific Computing: Manno, Switzerland, 2000.
(59) Gonzalez, C.; Schlegel, H. B. *J. Phys. Chem.* **1990**, *94*, 5523–5527.
(60) Baboul, A. G.; Curtiss, L. A.; Redfern, P. C.; Raghavachari, K. *J. Chem. Phys.* **1999**, *110*, 7650–7657.
(61) Scott, A. P.; Radom, L. *J. Phys. Chem.* **1996**, *100*, 16502.
(62) Li, Z. J.; Singh, S.; Woodward, W.; Dang, L. *J. Phys. Chem. A* **2006**, *110*, 12150.
(63) Kramp, F.; Paulson, S. E. *J. Phys. Chem. A* **1998**, *102*, 2685.
(64) Behnke, W.; Hollander, W.; Koch, W.; Nolting, F.; Zetzsch, C. *Atmos. Environ.* **1998**, *22*, 1113.
(65) Colomb, A.; Jacob, V.; Kaluzny, R.; Baussand, R. *Int. J. Chem. Kinet.* **2004**, *36*, 367.
(66) Coeur, C.; Jacob, V.; Foster, P.; Baussand, R. *Int. J. Chem. Kinet.* **1998**, *30*, 497.
(67) Aschmann, S. M.; Arey, J.; Atkinson, R. *J. Phys. Chem. A* **2001**, *105*, 7598.
(68) Kwok, E. S. C.; Atkinson, R. *Atmos. Environ.* **1995**, *29*, 1685.
(69) Atkinson, R. *Atmos. Chem. and Phys.* **2003**, *3*, 2233.
(70) Krasnoperov, L. N.; Michael, J. V. *J. Phys. Chem. A* **2004**, *108*, 5643.

JP810987U